Untangling mechanisms of crude oil toxicity in a cold water fish via gene expression, morphology and PAHs at two developmental stages

Elin Sørhus[1], Carey E. Donald[1], Denis da Silva[2], Anders Thorsen[1], Ørjan Karlsen[1] and Sonnich Meier[1]

[1]Insititue of Marine Research, Bergen, Norway

[2]Northwest Fisheries Science Center (NOAA), 2725 Montlake Blvd. East, Seattle, WA 98112-2097, USA

Abstract

Early life stages of fish are highly sensitive to crude oil exposure and thus, short term exposures during critical developmental periods could have detrimental consequences for juvenile survival. To obtain a broader understanding of the mechanisms behind crude oil toxicity, we administered crude oil to Atlantic haddock (*Melanogrammus aeglefinus*) in short term (3-day) exposures at two developmental time-points, before and after onset of heartbeat. A frequent sampling regime enabled us to determine and link immediate PAH uptake, metabolite formation and gene expression changes (*cyp1a,b,c,d*, *bmp10*, *abcb1* and *rhag*). In general, the embryotoxic consequences were more severe in the earliest exposure, and oil droplet fouling enhanced the toxicity. This study detected circulation-independent, oil-induced gene expression changes and separated phenotypes linked to proliferation, growth and disruption of formation events at early and late developmental stages. A greater understanding of crude oil toxicity is essential for predicting the consequences of oil spills.

Graphical abstract

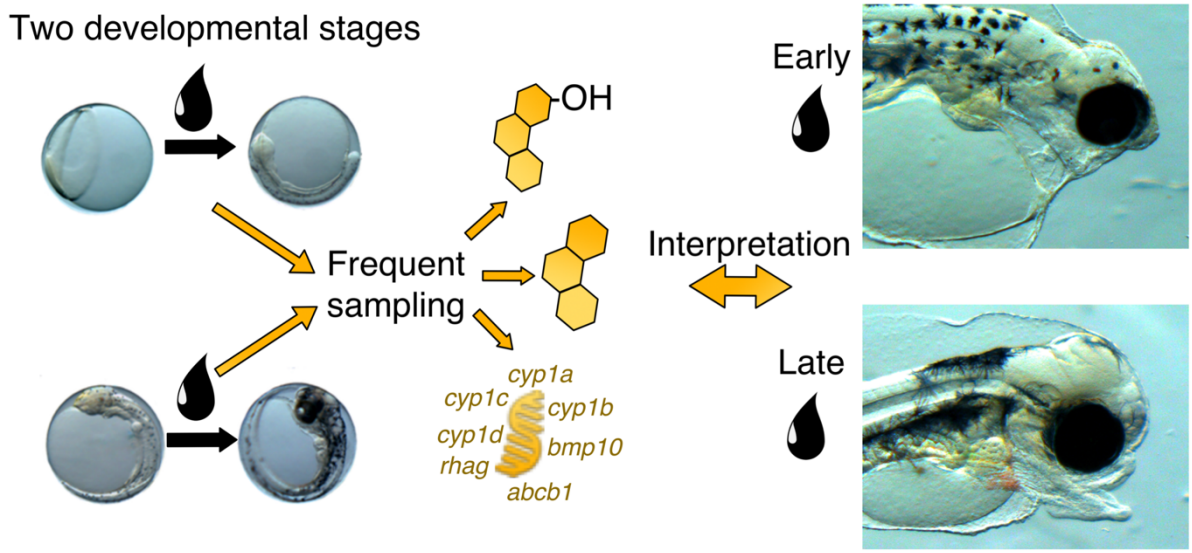

Highlights

- Oil droplet fouling occurred in the whole water column and increased the oil toxicity.
- Early exposure resulted in higher PAH uptake due to lower metabolism resulting in more severe abnormalities.
- A rapid and circulation-indepenent regulation of *bmp10* suggested a direct oil-induced effect on calcium homeostasis.
- Expression of *rhag* indicated a direct oil-induced effect on osmoregulatory cells and osmoregulation.
- Severe eye abnormalities especially in the late exposure was linked to inappropriate overexpression of *cyp1b* in the eyes .

Key words

Crude oil exposure, PAH uptake and metabolism, gene expression, cyp1a, cyp1b, cyp1c, cyp1d, bmp10, abcb1, rhag, development, Atlantic haddock, cold-water marine fish, phenotypes, cardiotoxicity, craniofacial, phenanthrene metabolites

Introduction

Globally, fish habitats are frequently impacted by accidental oil spills. For fish, consequences of crude oil toxicity are stage dependent, and early life stages (eggs and larvae) are thought to be highly vulnerable for several reasons. Early life stages drift and have no opportunity to avoid contaminated areas compared to juvenile and mature fish (Carroll et al., 2018; Olsen et al., 2010). Relative content of lipids and surface-area-to-volume ratio are higher

in early life stages compared to juveniles/adults, making them more susceptible to accumulation of lipophilic environmental toxicants (Petersen and Kristensen, 1998). Finally, critical developmental processes like patterning and organogenesis can be disrupted by crude oil exposure (Incardona, 2017; Pasparakis et al., 2019; Sørhus et al., 2017). However, there are large interspecies sensitivity differences, e.g. the Atlantic haddock (*Melanogrammus aeglefinus*) embryo is approximately 10 times more sensitive to crude oil than its close relative Atlantic cod (Gadus morhua) due to oil droplet fouling on the haddock chorion (Sørensen et al., 2017).

Crude oil is a complex mixture of thousands of different components, however, the content of polycyclic aromatic hydrocarbons (PAHs) appears to correlate to the toxicity in developing fish (Adams et al., 2014; Carls and Meador, 2009). Deactivation and excretion of the larger PAHs (4-6 rings) is initiated by activation of the aryl hydrocarbon receptor (AhR), which in turn induces PAH-degrading enzymes, such as cytochrome P4501A (Cyp1a). Cyp1a induction has for a long time been used as a sensitive biomarker for crude oil toxicity (Goksøyr, 1995). The detoxification process is divided into three phases, with activation of substrate in phase I by *e.g.* cyp1a, followed by conjugation in phase II, and finally transport and excretion in phase III (Wells et al., 2009). Although PAHs are themselves toxic, reactive intermediates (reactive oxygen species, ROS) created during the detoxification process can cause toxicity such as oxidative damage to cellular macromolecules and disruption of signal transduction (Wells et al., 1997).

Cardiac morphology abnormalities can be a result of AhR-dependent mechanisms (Wells et al., 1997), circulation abnormalities (Andres-Delgado and Mercader, 2016) and direct disruption of signaling pathways, i.e calcium (Ebert et al., 2005; Rottbauer et al., 2001; Sørhus et al., 2017). In addition, tricyclic PAHs are shown to cause cardiotoxicity through an AhR-independent manner (Incardona et al., 2004; Marris et al., 2019). Tricyclic PAHs are poor inducers of AhR, and instead act by blocking the repolarizing potassium efflux and a reduction in intracellular calcium cycling (Brette et al., 2014; Brette et al., 2017). The disruption of ionic signaling leads to defects in cardiac rhythm and contractility (Incardona, 2014; Incardona et al., 2009; Sørhus et al., 2016b) as well as calcium regulated cardiomyocyte proliferation (Ebert et al., 2005; Huang et al., 2012; Rottbauer et al., 2001; Sørhus et al., 2017). Beyond these circulatory defects that affect cardiac development (Andres-Delgado and Mercader, 2016), other extra-cardiac abnormalities can be secondary to circulatory defects, including craniofacial and eye development, and osmoregulatory and lipid metabolism deficiencies (Incardona et al., 2004; Incardona and Scholz, 2016; Laurel et al., 2019; Sørhus et al., 2017; Sun et al., 2019)

Numerous other pathways/endpoints have also been reported beyond the effects downstream of circulatory defects described above. PAH-related disruption of retinoid signaling interrupts eye development (Lie et al., 2019). Craniofacial development and growth can be disrupted by inappropriate signaling in formation processes like midline signaling (Abramyan, 2019; Delling et al., 2013; Kimmel et al., 2001) or secondary to impact on craniofacial muscle apparatus (Shwartz et al., 2012). Severe oil-induced aberrations lead to early larval mortality, yet even the smaller developmental impacts can affect survival later in life (Heintz et al., 2000; Hicken et al., 2011). Recently, a study linked oil-induced changes in lipid composition and dynamics to reduced growth and survival in polar cod (*Boreogadus saida*) (Laurel et al., 2019). Consistently, impacts on lipid metabolism pathways have been reported in several RNAseq studies (Sørhus et al., 2017; Xu et al., 2017). Several gene expression studies have started to unravel initiating events and key events of adverse outcome pathways of crude oil (Laurel et al., 2019; Lie et al., 2019; McGruer et al., 2019; Sørhus et al., 2017), but there are still knowledge gaps in understanding the underlying mechanisms of crude oil toxicity.

In this study we aim to improve our understanding of cause and effect relationships by linking immediate transcriptional changes to morphological phenotypes, PAH uptake and metabolism. A frequent and thorough sampling regime during and after exposure enabled us to detect immediate changes. We focused specifically on genes found interesting in a previous study (Sørhus et al., 2017) that are involved in various parts of development and function: cardiac development and calcium homeostasis, osmoregulation and ammonium waste excretion, transport of xenobiotic products, and enzymes possibly involved in phase I xenobiotic metabolism.

This study was designed to understand key events of adverse outcome pathways. First, exposure at the early embryonic stage prior to first heartbeat (2.5-5.5 days post-fertilization (dpf)) allowed us to detect circulation-independent, oil-induced gene expression changes. Second, exposure both during and after completion of organogenesis (7.5-10.5 dpf) enabled us to separate phenotypes linked to proliferation, growth and disruption of formation events at early and late developmental stages. Finally, increased knowledge about uptake, induction and rate of PAH metabolism helps to pinpoint sources of crude oil toxicity. A greater understanding of crude oil toxicity in the framework of adverse outcome pathways is essential for predicting more accurately both acute and delayed consequences of accidental and operational oil spills.

Materials and methods

Animal collection, maintenance and exposure set up

Fertilized Atlantic haddock (*Melanogrammus aeglefinus*) eggs were collected from tanks with wild-caught broodstock haddock maintained at the Institute of Marine Research, Austevoll Research station. The fertilized eggs were kept in indoor incubators (8±1°C), until transfer of ≈5000 eggs to 50 L green polytethylene plastic experimental tanks. Flow through in the tanks was set to 32 L/hr, the water temperature 8.0°C, and light regime was 12 hours light, 12 hours dark provided by broad spectrum 2x36W Osram Biolux 965 (Osram GmbH, Munich, Germany).

The crude oil used was a weathered blend from the Heidrun oil field of the Norwegian sea. The crude oil is representative of the oil found in Lofoten island areas, an area of both haddock spawning and potential oil industry development. The exposure regime was identical to previous studies (Sørhus et al., 2016b).

Two short (72 hours) exposure experiments were performed, hereafter referred to as *early* and *late* exposure (Fig. 1A). The *early* exposure started at 2.5 dpf and ended at 5.5 dpf (10% epiboly to 10-20 somite/cardiac cone stage), while the *late* exposure started at 7.5 dpf and ended at 10.5 dpf (30-40 somite stage to hatching gland stage). The experimental setup consisted of a control and three exposure doses in a total of 18 tanks (Fig. 1B): control (*C*) 0.0 µg oil/L; low (*L*) 30 µg oil/L; medium (*M*) 100 µg oil/L; and high 300 µg oil/L. In our previous oil exposure experiments with haddock embryos, eggs were allowed to float freely (Sørensen et al., 2017; Sørhus et al., 2015; Sørhus et al., 2016b). Haddock eggs have a natural high buoyancy which allocates them close to the surface, and are potentially exposed to any slick formation. Therefore, eggs were added to plankton mesh chambers (Fig. 1B) in four replicate tanks of each treatment and submerged into the water column (*sub*). To identify an effect of oil droplet binding at the surface, the high dose was administered in three ways: like the other doses, where the eggs were held submerged under the water surface (*H sub*); where the eggs were allowed to float at the surface (*H surf*); and where the eggs were allowed to float and the exposure water was filtered to remove oil microdroplets (water soluble fraction; *H WSF*).

After exposure, ≈1000 eggs were transferred to recovery flow through tanks with clean water where they were kept until termination of experiment at 3 days post-hatching (dph). Throughout this work, multiple terms are used to define timepoints, based on days post-fertilization (dpf), hours post-exposure start (hpes), and days post-hatching (dph) (Fig 1A).

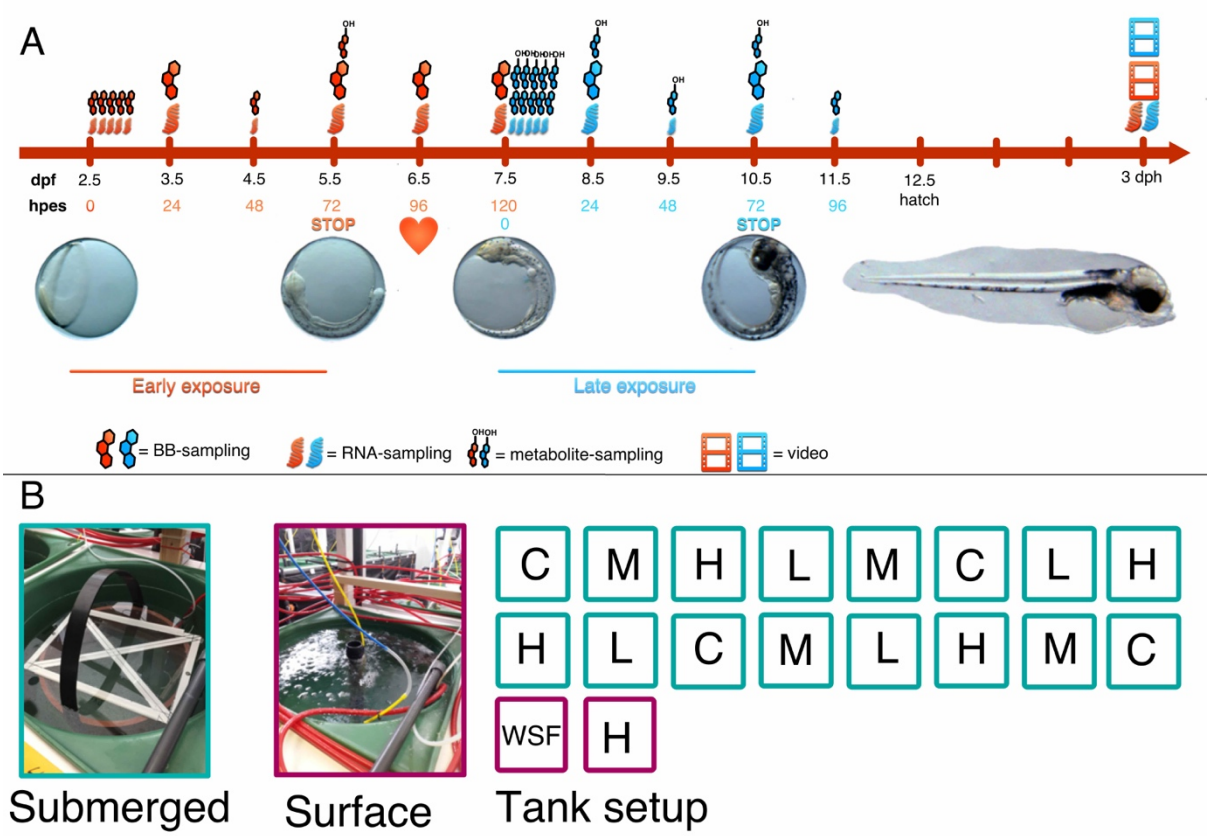

Figure 1: ***Experimental design and overview.*** *A) Timeline for experiments in relation to development. Atlantic haddock (Melanogrammus aeglefinus) embryos were exposed from 2.5 days post fertilization (dpf) to 5.5 dpf (early exposure) and from 7.5 dpf to 10.5 dpf (late exposure). Heart symbol indicates time point for observation of first heartbeat (6.5 dpf). Samplings were performed from 1-120 hours post exposure start (hpes) for the early exposure, and from 1-96 hpes for the late exposure. Videos were conducted 3 days post hatching (dph) for both experiments. Red and blue labeling of timepoints and sampling symbols represent early and late exposure, respectively. Small and large sampling symbols indicate sampling of high doses and control and sampling of all groups, respectively. B) Tank setup. C = control, L = Low dose, M = Medium dose, H = High dose, WSF = Filtered oil dispersion (water soluble fraction). The turquoise tanks were submerged.*

160 **Sampling regime**

161 Duplicate sample collection from all 18 tanks for total RNA extraction, body burden
162 and metabolites occurred at 24, 72 hpes and 3 dph for both experiments, as well as 96 and 120
163 hpes for the *early* exposure. A more thorough time series with triplicate samples was collected
164 from a tank of each of four selected treatments (*C*, *H sub*, *H surf* and *H WSF*) following the
165 sampling regime described in Fig. 1A, with sampling points at 1, 2, 4, 8, 12, 24, 48, 72, 96 and
166 120 hpes. Fewer replicates were taken for *H surf* and *H WSF* at some of the latest time points
167 due to high mortality. The precise number of eggs in each sample pool was counted from
168 microscope pictures.

169

170 **Analytical chemistry**

171 *PAH analysis in exposure water and body burden samples*

172 Water samples (1 L) were taken from each exposure tank at the beginning and the end
173 of each experiment, preserved by acidification (HCl, pH < 2) and then stored at 4 °C in the dark
174 until further handling. Details are given in Sørensen et al. (2017). In short, the water samples
175 were extracted twice by partitioning to dichloromethane (30 mL) in a separatory funnel (2 min).
176 Deuterated internal standards (naphthalene-d8, biphenyl-d8, acenaphtylene-d8, anthracene-
177 d10, pyrene-d10, perylene-d12 and indeno[1,2,3-c,d]perylene-d12) were added prior to
178 extraction to account for analyte~~s~~ loss during extraction. The combined extracts were
179 concentrated by solvent evaporation prior to analysis by GC-MS. The following PAH
180 compounds were measured: C0-, C1-, C2-, C3-, C4-naphthalenes (NAP), anthracene (ANT),
181 acenaphthylene (AC), acenaphtene (AE), C0-, C1-, C2-, C3-fluorene (FLU), C0-, C1-, C2-, C3,
182 C4-phenanthrene/anthracenes (PHE), C0-, C1-, C2-, C3-, C4-dibenzothiophenes (DBT),
183 fluoranthene (FL), C0-, C1-, C2-, C3-pyrene (PYR), benzo[a]anthracene (BAA), C0-, C1-, C2-
184 , C3, C4-chrysene (CHR), benzo[b+j+k]fluoranthene (BKF), benzo[e]pyrene (BEP),
185 benzo[a]pyrene (BAP), perylene (PER), benzo[g,h,i]perylene (BP), indeno[1,2,3-c,d]pyrene
186 (IND) and dibenzo[a,h]anthracene (DBA).

187 Samples for PAH body burden were collected frequently (Fig. 1A) to detect immediate
188 changes in PAH uptake. The 48 hpes time point for the *late* exposure was compromised during
189 analysis and data are not available. Each sample collected consisted of 50-100 pooled animals
190 preserved by flash-freezing in liquid nitrogen and stored at −80 °C. Tissue samples were
191 extracted by solid-liquid extraction and cleaned-up by solid phase extraction (SPE) prior to
192 analysis. The method is described in detail in Sørensen et al. (2017). Briefly, after addition of

193 internal standards the samples were homogenized in 2 mL dichloromethane-hexane (1:1, v/v),
194 followed by addition of sodium sulphate (150 mg) and two rounds of vortex extraction (30 sec)
195 and centrifugation (2000 rpm, 2 min). The combined organic extract was concentrated to ~1 mL
196 prior to clean-up by SPE (Agilent Bond Elut SI, 500 mg). The SPE columns were conditioned
197 with hexane and the extract eluted with 6 mL 10% dichloromethane in hexane. The purified
198 extract was concentrated to 100 µL under a gentle stream of N_2.
199 Water and body burden samples were analyzed on an Agilent 7890 gas chromatograph
200 coupled to an Agilent 7010c triple quadrupole mass detector (GC-MS/MS) as described
201 previously in Sørensen et al. (2017). For the body burden samples, a matrix-matched calibration
202 was used, made from the blank extraction of haddock and cod eggs.

203 *Phenatharene metabolite analysis in haddock eggs*

204 There are today no analytical methods that are able to detect the whole metabolome of
205 PAH in fish (Beyer et al., 2010). In the present study we have included detection of phenathrene
206 metabolites as representatives of complex PAH metabolism. We analyzed the main products of
207 phenathrene metabolism in fish which are dominated by dihydroxylated-phenanthrene together
208 with minor levels of monohydroxylkated-phenanthrenes (Goksoyr et al., 1987; Pampanin et al.,
209 2016; Pangrekar et al., 2003; Sette et al., 2013).

210 The following standards of target compounds were purchased from Chiron AS
211 (Trondheim, Norway): 1-hydroxyphenanthrene (1-OH-PHE), 2-hydroxyphenanthrene (2-OH-
212 PHE), 3-hydroxyphenanthrene (3-OH-PHE), 4-hydroxyphenanthrene (4-OH-PHE), 9-
213 hydroxyphenanthrene (9-OH-PHE) , *trans*-9,10-dihydroxy-9,10-dihydrophenanthrene (9,10-
214 diol-PHE) and surrogate standard 2-hydroxynaphthalene-d7 (2-OH-NPH-d7). The standard
215 *trans*-1,2-dihydroxy-1,2-dihydrophenanthrene (1,2-diol-PHE) was purchased from MRI
216 Global Carcinogen Repository (Kansas City, MO, USA) . Samples for metabolite analysis were
217 collected at 72 hpes in *early* exposure and 1-72 hpes in *late* exposure (Fig. 1A), flash frozen
218 and kept at -80 °C until analysis. Between 50-100 eggs pooled from the same treatment were
219 homogenized and a 50 µL aliquot of the homogenized mixture was diluted with water to 200
220 µL and spiked with surrogate standard. The homogenate was then added to phospholipid
221 removal cartridges (Phenomenex Phree cartridges) contaning methanol and eluted under
222 vacuum to remove phospholipids and proteins, followed by enzymatic hydrolysis by adding a
223 pH-5 buffer containing 2000 U of β-glucuronidase/sulfatase (Sigma-Aldrich) and incubating
224 for 1 hour at 40 °C. The hydrolysis reaction was then suspended with the addition of glacial

225 acetic acid. We used SPE with Strata-X 200 mg/6 mL cartridges (Phenomenex Inc.) pre-
226 conditioned with methanol and distilled water. Sample was added and washed with water and
227 63:37 methanol:water (v/v) before drying 30 minutes under vacuum. Target metabolites were
228 finally eluted using 65:35 methanol:diethyl ether (v/v). Final volume was reduced to 3 mL
229 before addition of internal standards and an aliquot was transferred for final analysis of the
230 PAH metabolites.

231 Instrumental analysis was performed with a Waters Acquity high performance liquid
232 chromatograph (LC) coupled with an AB Sciex QTRAP 5500 tandem mass spectrometer (MS)
233 operating in negative electrospray ionization mode with ion spray voltage of 4500 V and
234 multiple reaction mode (MRM) with the source temperature at 650 °C. The LC was equipped
235 with a 0.2-µm pre-filter followed by a 2.1 x 5.0 mm (1.7-µm particle size) reversed phase guard
236 column (BEH Shield RP18, Waters Co) and a 2.1 x 150 mm (1.7 µm particle size) reversed-
237 phase column (BEH Shield RP18, Waters Co). Water (solvent A) and methanol (solvent B)
238 were used as a mobile-phase with a 29-minute linear gradient as follows (solvent A/solvent B):
239 initial gradient was 50/50 at 0.2 mL/min; 15 min to 20/80 at 0.2 mL/min; 0.1 min to 100%
240 solvent B and 0.1 min to 0.3mL/min; held at 100% B for 6.8 min at 0.3 mL/min; 0.5 min to
241 return to initial gradient 50/50 at 0.3 mL/min; held at 50/50 for 6.0 min at 0.3 mL/min; 0.1 min
242 to 0.2 mL/min and kept for 0.4 min. The column temperature was maintained at 45ºC.

243 Sum OHPHEs (ΣOHPHEs) is the sum concentrations of 1-OH-PHE, 2-OH-PHE + 3-
244 OH-PHE (estimate concentration, as these are chromatographically co-eluting isomers), 4-OH-
245 PHE and 9-OH-PHE. Sum PHE-diols (ΣOHPHEs) is the sum concentration~~s~~ of 1,2-diol-PHE
246 and 9,10-diol-PHE. Sum PHE metabolites (Σ PHE metabolites) is the sum concentration~~s~~ of all
247 metabolites measured. The quantitative results were converted from ng metabolites/embryo to
248 ng/g by using average mass of one haddock egg (0.00218 g).

249

250 **Detection of Cyp1a activity**

251 Ethoxyresorufin-O-deethylase (EROD) assay was applied to detect Cyp1a activity.
252 Activity was measured at 72 hpes (5.5 dpf) in the *early* exposure. The embryos were at the end
253 of Organogenesis 1, at the 10-30 somite/cardiac cone developmental stage (Fridgeirsson, 1978;
254 Hall et al., 2004; Sørhus et al., 2016a). The procedure was performed as described in Gonzalez-
255 Doncel et al. (2011). Briefly, 7-ethoxyresorufin (7ER) was added to live embryos and the
256 Cyp1a-catalyzed fluorescing product, resorufin, was detected with fluorescence microscopy. A
257 stock of 7ER (48 mg 7ER/L) (Sigma-Aldrich, Germany) was made in 100% DMSO (Thermo

258 Fisher Scientific). Control, DMSO and crude oil exposed embryos were transferred to 24-well
259 plates where they were incubated in the dark for 1 hour in 20 µg 7ER/L or DMSO in sterile sea
260 water. After exposure the solution was drained off and exchanged with sterile sea water. Images
261 of 12-20 embryos per treatment were captured with a digital camera (SPOT Insight 5 Mpx)
262 coupled to a Nikon AZ100 fluorescence microscope. For each set of embryos, two fluorescence
263 images were captured using the rhodamine filter (Ex 545/25 nm and Em 605/70 nm) to detect
264 EROD activity and DAPI filter (Ex 350/50 nm and Em 460/50 nm) to detect the internal
265 fluorescence of PAH compounds. In addition, a corresponding brightfield image was captured
266 for each set of fluorescence. Exposure time and gain for all fluorescence images were set at 300
267 ms and 4 g. Semi-quantitative measurements of EROD fluorescence in the embryos was
268 estimated using the adjusted light intensity in the whole egg in the various treatments. Adjusted
269 light intensity was measuered using ImageJ software (Schneider et al., 2012;
270 http://imagej.nih.gov/ij/, 1997–2016) and was calculated using the following formula: Adjusted
271 light intensity = (light intensity in Treatment with 7ER)/(light intensity in Treatment with
272 DMSO).
273
274 **Imaging of live embryos/larvae and measurements of cardiac function**
275 Images were taken at all sampling points to define developmental stage, morphological
276 abnormalities and degree of oil droplet accumulation. At 3 dph, all groups were imaged to
277 assess morphological and cardiac functional endpoints. Images were collected for all exposure
278 tanks in both *early* and *late* exposures. Digital still micro-images and 20-second videos of live
279 3 dph larvae were obtained using an Olympus SZX-10 Stereo microscope equipped with a 1.2
280 megapixel resolution video camera (Unibrain Fire-I 785c) controlled by BTV Pro 5.4.1
281 software (www.bensoftware.com). Image calculations were calibrated with a stage micrometer.
282 Animals were immobilized in a glass petri dish filled with 3 % Methylcellulose (Sigma-
283 Aldrich, Germany) in seawater and kept at 8°C using a temperature-controlled microscope stage
284 (Brook Industries Inc. Lake Villa, IL. USA). Length of ethmoid plate, mandible, area of edema
285 and length, systolic and diastolic diameter of ventricle and atrium were measured using ImageJ
286 (Schneider et al., 2012; http://imagej.nih.gov/ij/, 1997–2016) with the ObjectJ plugin
287 (https://sils.fnwi.uva.nl/bcb/objectj/index.html) from images as described previously (Sørhus et
288 al., 2016b). Additionally, eye diameter was quantified, and eye shape and deformities were
289 described according to categories: normal shape (no), bend shape (be), irregular shape (irr),
290 protruding lens (pl). Six distinct craniofacial phenotypes were identified. Degree of looping of
291 heart was also described (normal looping (n), poor looping (p) and severly poor looping (sp)).

292 The area occupied by edema fluid was quantified as the difference between the total area of the
293 yolk sac and the area of the yolk mass, expressed as a percentage of total yolk sac area.
294 Similarly, ventricular and atrial diastolic (D) and systolic diameter (S) were used to estimate
295 the fractional shortening (FS = (D − S)/D). Measurements from both images and videos were
296 performed blind.
297
298 **Oil induced gene expression changes**
299 All animals collected for RNA extraction were frozen in liquid nitrogen and stored at
300 −80 °C after being imaged (as described in the previous section). Total RNA was extracted
301 from frozen pools with 10 eggs/larvae with Maxwell HT simplyRNA (Promega corporation)
302 according to the manufacturer's instructions using Biomek 4000 Automated liquid handler
303 (Beckman coulter). Quantity and quality of the extracted total RNA was checked using
304 Nanodrop spectrophotometer (NanoDrop Technologies, Wilmington, DE, USA) and
305 Bioanalyzer (Agilent Technologies, Santa Clara, CA, USA) respectively. cDNA was
306 subsequently generated using SuperScript VILO cDNA Synthesis Kit (Life Technologies
307 Corporation), according to the manufacturer's instructions, and was normalized to obtain a
308 concentration of 50 ng/µL. The described frequent sampling regime was followed to detect
309 immediate gene expression changes (Fig. 1A and see the previous section *"Sampling regime"*).
310 Specific primers and probes for real-time qPCR analysis of Atlantic haddock were
311 designed with Primer Express software (Applied Biosystems, Carlsbad, California, USA)
312 (*cyp1a* and the technical reference *ef1a)* or Integrated DNA Technology (IDT) probe and
313 primer design software (IDT Inc., Iowa, USA) (*cyp1b, cyp1c, cyp1d, abcb1, rhag* and technical
314 reference *rxrba*), according to the manufacturer's guidelines. Primer and probe sequences are
315 given in Supplementary table S1. Real-time qPCR assays were performed in duplicate, using
316 384-well optical plates on a QuantStudio 5 Real Time PCR System (Thermofisher Scientific)
317 with settings as follows: 95 °C for 20 s, followed by 40 cycles of 95°C for 1 s and 60°C for 20
318 s. Duplicates with standard deviation[2] ($SD^2 \geq 0.05$ were either rerun or eliminated from the
319 dataset. No-template control, reverse transcriptase enzyme control and genomic DNA controls
320 were included. For each 5 µl PCR reaction, a 1.5 µl cDNA 1:40 dilution (1.9 ng) was mixed
321 with 200 nM fluorogenic probe, 900 nM sense primer, 900 nM antisense primer in 1xTaqMan
322 Fast Advanced Master Mix (Applied Biosystems, Carlsbad, California, USA). Gene expression
323 data were calculated relative to control in the first sampling point using the ΔΔΔCt method
324 generating reference residuals from *ef1a* and *rxrba*, as described in detail in Edmunds et al.
325 (2014).

Localization of *rhag* gene expression

Location of *rhag* gene expression was examined using a method derived from previous protocols (Hall et al., 2003; Thisse and Thisse, 2008; Valen et al., 2016). We performed whole mount *in situ* hybridization on unexposed 10 dpf embryos to determine location of *rhag* in early life stages of fish. Detailed protocol can be found in Supplementary information.

Statistics

Statistical differences in Cyp1a activity, morphology, cardiac function, PAH water concentration, PAH body burden, and OHPAH metabolites were tested using one-way ANOVA with Dunnet´s multiple comparison in R (The R Foundation for Statistical Computing Platform). In the gene expression data, statistically significant differences were tested using both One-way and Two-way ANOVA with Dunnet´s multiple comparison in R. ~~for.~~ PAH water concentration, PAH body burden, OHPAH metabolites and gene expression data were log-transformed due to large differences in levels and thus standard deviation. In craniofacial and eye phenotypes and appearance of silent ventricle, statistical differences between treatments and control were evaluated using chi-square test. Statistical difference was denoted $p<0.05$ (*), $p<0.01$ (**), $p<0.001$ (***). Error bars in all figures represent the standard deviation of the mean.

Ethics statement

The animals were monitored daily, and any dead larvae were removed. All sampled embryos and yolk sac larvae were euthanized immediately in liquid nitrogen. The Austevoll Aquaculture Research station has the following permission for catch and maintenance of adult Atlantic haddock: H-AV 77, H-AV 78 and H-AV 79. These are permits given by the Norwegian Directorate of Fisheries. Furthermore, the Austevoll Aquaculture Research station has a permit to run as a Research Animal facility using fish (all developmental stages), with code 93 from the national IACUC; NARA, although no approval is necessary to perform studies with fish embryos and yolk sac larvae.

Results

Overall, both *early* and *late* exposure resulted in functional and morphological abnormalities, but they were more severe in the *early* exposure. Tissue uptake of PAHs was

360 higher in the *early* exposure, followed by a stronger, but delayed *cyp1a* induction. The *H WSF*
361 group showed very few oil induced abnormalities in both exposures. Gene expression patterns
362 were unique between *early* vs *late* exposures.
363
364 **Oil droplet fouling in surface and submerged embryos**
365 Oil droplet fouling was observed on embryos in both submerged (*L, M, H sub*) and
366 surface (*H surf*) exposures regardless of timing, and was evident after only 1 hour of exposure
367 (Fig 2A and B, top panels). The oil droplet fouling effect was higher in the surface (*H surf*)
368 exposure due to the accumulation of oil microdroplets on the surface (Fig. 2). While oil droplets
369 in the *early* exposure were distributed all over the surface, the *late* exposure embryos mainly
370 accumulated oil droplets at one area on the chorion (Fig 2B, filled black arrows). In the filtered
371 high dose group (*H WSF*), no oil droplets were detected on the chorion (Fig 2A and B, right
372 panel). After transfer to clean water, some of the droplets were washed off, however, in addition
373 to a reduced number of apparent oil droplets (brown), translucent droplets were now visible on
374 the surface (white arrow head Supplementary Fig. S1). This phenomenon was not observed in
375 the *late* exposure due to hatching that occurred shortly after end of exposure (11 dpf).

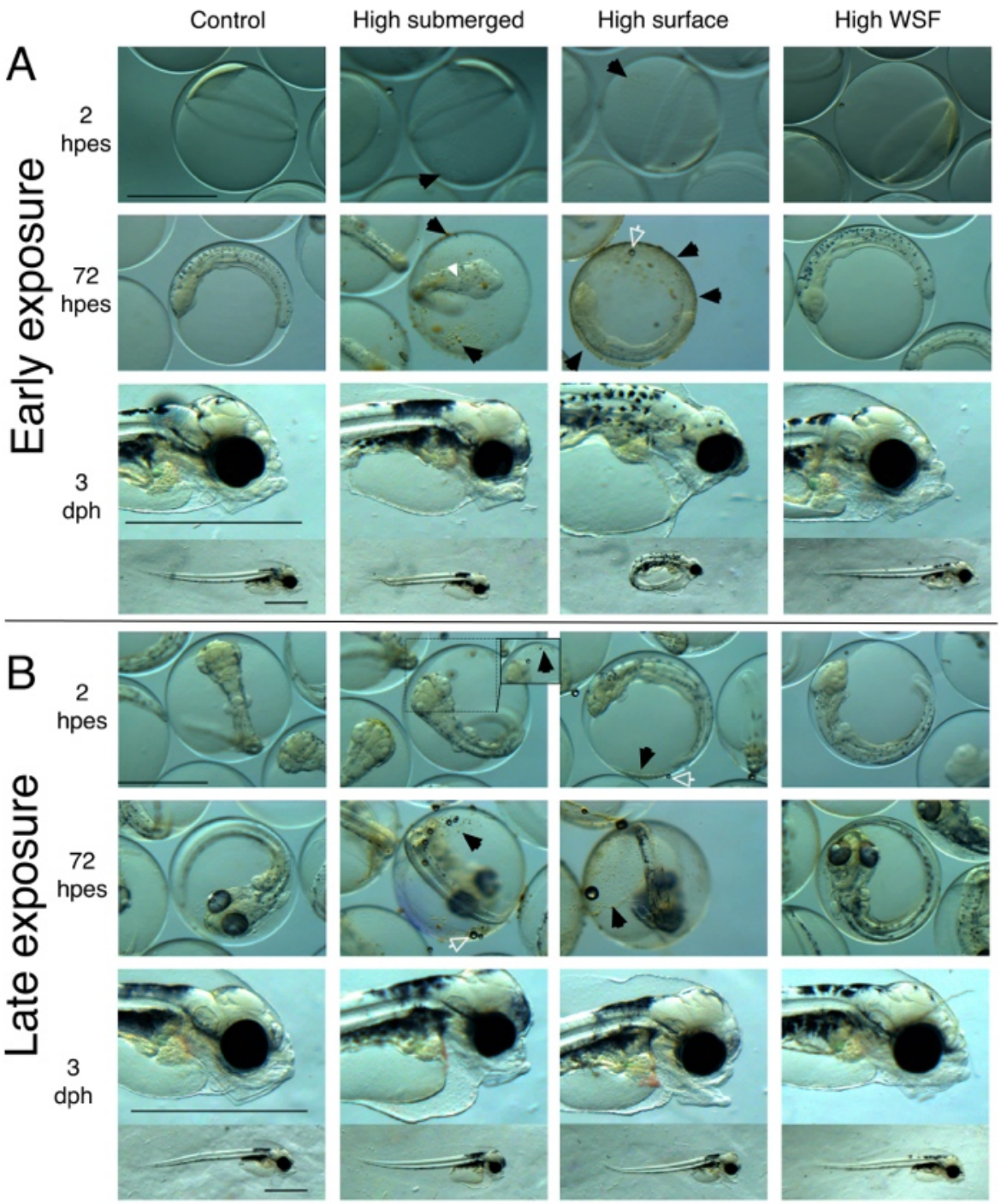

Figure 2: ***Oil droplet fouling and morphology.*** *A) early and B) late embryonic exposure of Atlantic haddock. Top panels show 2 hours post exposure start (hpes), middle panels 72 hpes (exposure stop) and lower panels display representative phenotypes at 3 days post hatching (dph). Black arrows : oil droplets. White arrow head: indicates cardiac cone. White open arrow: air bubble trapped on the chorion. WSF: water soluble fraction.*

Scale bar: 1000 µm.

Oil exposure and PAH uptake

We successfully delivered doses of dispersed crude oil to the exposure tanks during the experiments. Total PAHs (dissolved and droplet associated) were monitored at the beginning and end of each exposure experiment (Fig. S2) . The water concentration of PAH was lower in the *H WSF* than the other high dose groups, and reflected the PAH contribution from the oil droplets. There were some differences in the total PAH concentration between the two experiments, but there were ~~a~~ clear gradients among the different treatment in both studies: total PAH concentration (µg PAH/L): Average (start and stop) concentrations after *Early* exposure *C* = 0.04 +/- 0.01, *L* = 0.47 +/- 0.61, *M* = 2.3 +/- 2.4, *H sub* = 5.2 +/- 1.7, *H surf* = 6.4 +/- 0.8 , *H WSF* = 3.7 +/- 1.0. *Late* exposure C = 0.04+/-0.01, L = 0.5+/-0.2, M = 2.2+/-0.8, *H sub* = 9.7 +/- 2.7 *H surf* = 8.3 +/- 2.9, *H WSF* = 6.3 +/-0.9

An immediate and prominent uptake of PAHs into the embryo was detected (Fig. 3). Body burden measurements of all doses at all time-points in both experiments had statistically significant elevated levels of PAH compared to control. Average total PAH tissue concentrations in the exposed groups for *early* exposure ranged from 38 (1 hpes, *H WSF*) to as high as 7800 ng/g ww (72 hpes, *H surf*). Values in the *late* exposure were between 75 (24 hpes, *L)* and 3000 ng/g ww (72 hpes, *H surf*). Notably, despite higher water concentrations in the *late* exposure, the highest tissue concentrations were found in the *early* exposure. Moreover, the tissue concentration in the *early* exposure peaked at a later time point than in the *late* exposure (72 hpes vs 24 hpes). The levels in the *H WSF* groups (in which the water was filtered) were more similar to the medium group, despite sharing the same oil content of the high dose (300 µg oil/L) (Fig. 3A). Figure 3B shows the profile of PAHs at 72 hpes, where, notably, the high molecular weight (HMW) PAH group (inset in Fig. 3B) found in medium, *H sub* and *H surf* groups, was lacking in the *H WSF* group. These HMW PAHs, *e.g.* PYRs and CHRs, accumulated substantially more in the *H surf* than in other groups. In addition, in the *H surf*, the levels of these HMW PAHs were up to four times higher in *early* vs *late* exposure (Fig. S3). Detailed profiles for individual PAHs at each time point are documented in Supplementary Dataset S1.

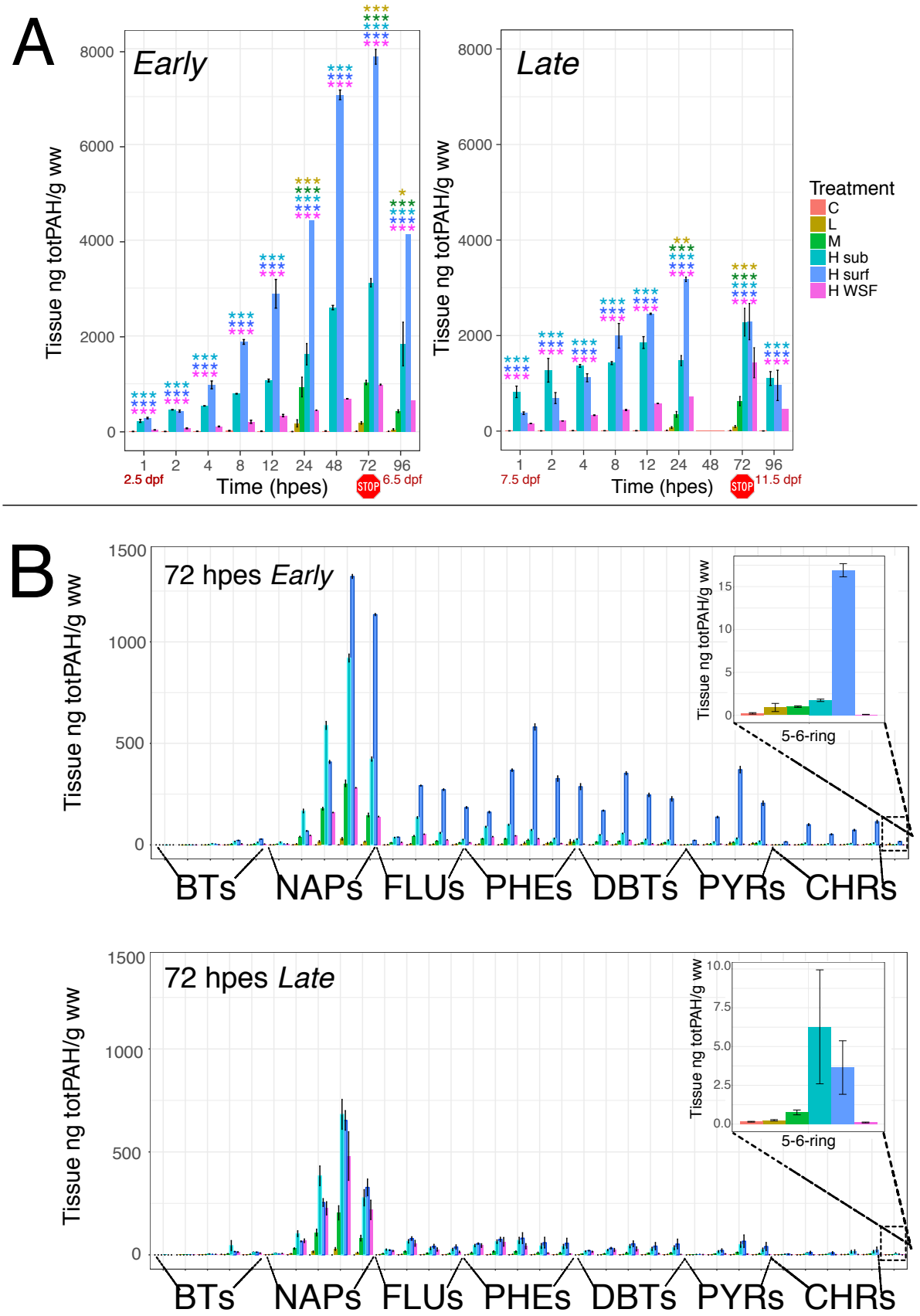
A
Early
Late
Tissue ng totPAH/g ww
Time (hpes)
2.5 dpf
6.5 dpf
7.5 dpf
11.5 dpf
STOP
Treatment
C
L
M
H sub
H surf
H WSF
B
72 hpes Early
72 hpes Late
5-6-ring
BTs
NAPs
FLUs
PHEs
DBTs
PYRs
CHRs

412

Figure 3: ***Tissue uptake of polycyclic aromatic hydrocarbons (PAHs).*** *A) Total body burden of PAHs from 1-96 hours post exposure start (hpes) in early (Left panel) and late (right panel) exposure. Exposure stop was after 72 hours. Statistical difference from control was tested at each time point with One-way ANOVA and significant differences are indicated by **=p<0.01 or ***: p<0.001. Note, at 96 hpes only one replicate from H surf and H WSF (early exposure) and H WSF (late exposure) were analyzed. B) PAH profile at exposure stop (72 hpes) in early (left panel) and late (right panel) exposure. Inset: magnification of 5-6 ring distribution in the treatment groups. Dpf: days post exposure, C: control, L: low dose, M: medium dose, H sub: high dose submerged, H surf: high dose surface, H WSF: high dose water soluble fraction, BTs: Benzothiophenes , NAPs: Naphtalenes, FLUs: Fluorenes, PHEs: Phenanthrenes, DBTs: Dibenzothiophenes, PYRs: Pyrenes, CHRs: Chrysenes.*

Hydroxylated phenanthrene metabolites

Hydroxylated phenanthrene metabolites were analyzed in the control and three high dose groups (*H sub*, *H surf* and *H WSF*) at *early* (only at exposure stop, 72 hpes) and *late* exposure (1-72 hpes). Metabolites assessed are presented as sum of monohydroxyphenanthrenes (ΣOHPHE) and sum of dihydrodiol phenanthrenes (ΣPHE-diols) (Fig. 4). Within these groups 1,2-diol-PHE was the dominating metabolite and accounted for approximately 90% of total detected metabolites (average of all treatments). Of the ΣOHPHE, 1-OH-PHE was the most abundant and contributed with 9% of the total metabolites (Supplementary Dataset S2).

Metabolite levels at exposure stop (72 hpes) for *early* exposure were approximately 3 times lower than *late* exposure (Fig 4A). In the *late* exposure, where we analysed for a metabolite profile over time, we observed significant levels of phenanthrene metabolites in all high dose groups after 24 hpes, and these levels continued to increase until exposure stop (Fig. 4B). The maximum body burden of PHE metabolites was found in the *H surf* group (72 hpes) in a concentration of 45 ~~56~~ ng/g ww, which is in the similar concentration ranges as the body burden of the parent PHE (95 ng/g ww found after 24 hpes). The metabolites in the *H WSF* were approximately 1/3 that of *H sub*, although they followed a similar trend over time. (Fig. 4B). The correlation between phenanthrene metabolites and body burden (Fig. 4C) demonstrates that the rate of biotransformation exceeds the rate of PAH uptake. By 12 hpes (*H sub*) and 24 hpes (*H surf*), the curve turns back on itself indicating that the formation of metabolites is increasing while the PAH body burden has begun to decrease (even under continuous exposure).

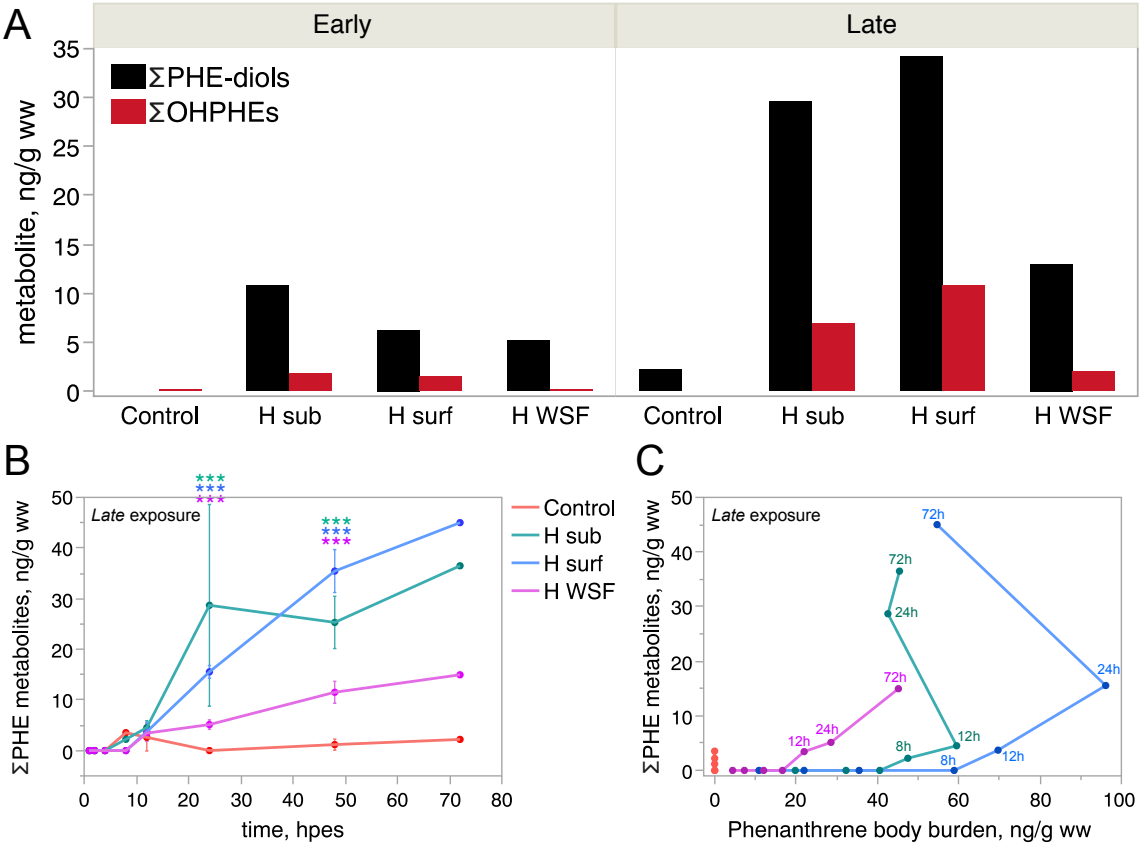

Figure 4: ***Tissue concentration of phenanthrene metabolites.*** *A) Concentrations of PHE-diols and OHPHEs at 72 hpes in early and late exposures (one sample per treatment). B) Concentrations of ΣPHE metabolites over time in late exposure. Statistical difference from control was tested at 12 hpes, 24, hpes and 48 hpes with one-way ANOVA with Dunnet's multiple comparison, and significant differences are indicated by ***: p<0.001. C) Sum of phenanthrene metabolites versus mean body burden of phenanthrene in late exposure. The backwards curve suggests that metabolism is faster than uptake towards the end of the exposure. H sub: high dose submerged, H surf: high dose surface, H WSF: high dose WSF.*

Temporal expression of *cyp1a, cyp1b, cyp1c* and *cyp1d* and EROD activity

Expression of *cyp1a* was immediate in both experiments. It was increasing throughout the *early* exposure (Fig. 5A),and the expression stayed steady from 12-72 hpes at the late exposure (Fig 5B). In the *early* exposure a 5- and 6- fold significant change of *cyp1a* was detected after 8 hours of exposure in *H sub* and *H surf*, respectively (Fig. 5A). All treatments at investigated time-points were up-regulated from 12 hpes (Fig. 5A). As with PAH body burden, the *cyp1a* expression in the *H WSF* group fell between the levels detected in low and medium dose in all

462 time points except at 120 hpes, which reflects the toxicity contribution of oil droplets in the
463 exposure that is reduced when the exposure water is filtered to yield the WSF exposure. In the
464 *late* exposure, the induction of *cyp1a* was much more rapid with 2 fold up-regulation after only
465 2 hours of exposure in the *H surf* group (Fig. 5B). From 8 hpes and onward significant up-
466 regulation of *cyp1a* was seen in all treatment groups including low and medium at 24 and 72
467 hpes (Fig. 5B). Similar to the *early* exposure, the *H WSF* group *cyp1a* expression fell between
468 levels detected in the medium and low dose groups (Fig. 5B).

469 Induction of *cyp1a* correlated with tissue uptake of PAH (Fig. S4). However, one of the
470 low dose tanks, L4, showed low PAH uptake and *cyp1a* induction in both *early* and *late*
471 exposures. It was therefore considered an outlier and eliminated for further analysis in both
472 experiments. Embryos from the L4 tank clustered to the control tanks rather than the low dose
473 tanks at both 24 hpes and 72 hpes (Fig. S5, 72 hpes).

474 The expression of the other *cyp1* paralogs, *cyp1b* and *cyp1c*, was delayed in the *early*
475 exposure and genereally followed the same pattern as *cyp1a* expression in the *late* exposure
476 (Fig. 5). The expression profile over time for the control group show a highly dynamic temporal
477 expression of *cyp1b, cyp1c* and *cyp1d* while *cyp1a* showed a stable expression throughout
478 embryonic development (Fig. S6A-D). In the early exposure, *cyp1c* was not appreciably
479 expressed regardless of treatment until 48 hpes (Fig. 5C) and at 72 hpes a developmentally
480 related 200 fold up-regulation in the control group was observed (Fig. S6). Similarly, a general
481 up-regulation of *cyp1b* was seen from 24 hpes, with a significant upregulation in surface dose
482 at the two latest time points (Fig. 5C). In comparison, at peak at 96 hpes *H surf* showed a 221
483 fold up-regulation of *cyp1a* while *cyp1b* and *cyp1c* showed a 2.5 fold and 82 fold up-regulation,
484 respectively, compared to control at 96 hpes. For *cyp1d*, almost no transcripts were detected at
485 any of the time points in either dose/control in the *early* exposure. In the *late* exposure *cyp1d*
486 was generally up-regulated at 72 hpes, with a significant up-regulation in *M* and *H sub* groups
487 (Fig. S7). After 10 days of recovery (*early* exposure) at 3 dph one of the groups *H surf*, still had
488 significant up-regulation of one of the *cyp1s*, namely *cyp1b* (Fig. S8A-D, left panel). While at
489 3 dph after 5 days of recovery (*late* exposure), significant up-regulation in *H surf* group was
490 observed for all *cyp1*s, and in *H sub* group for *cyp1a, b* and *c* (Fig. S8A-D, right panels).

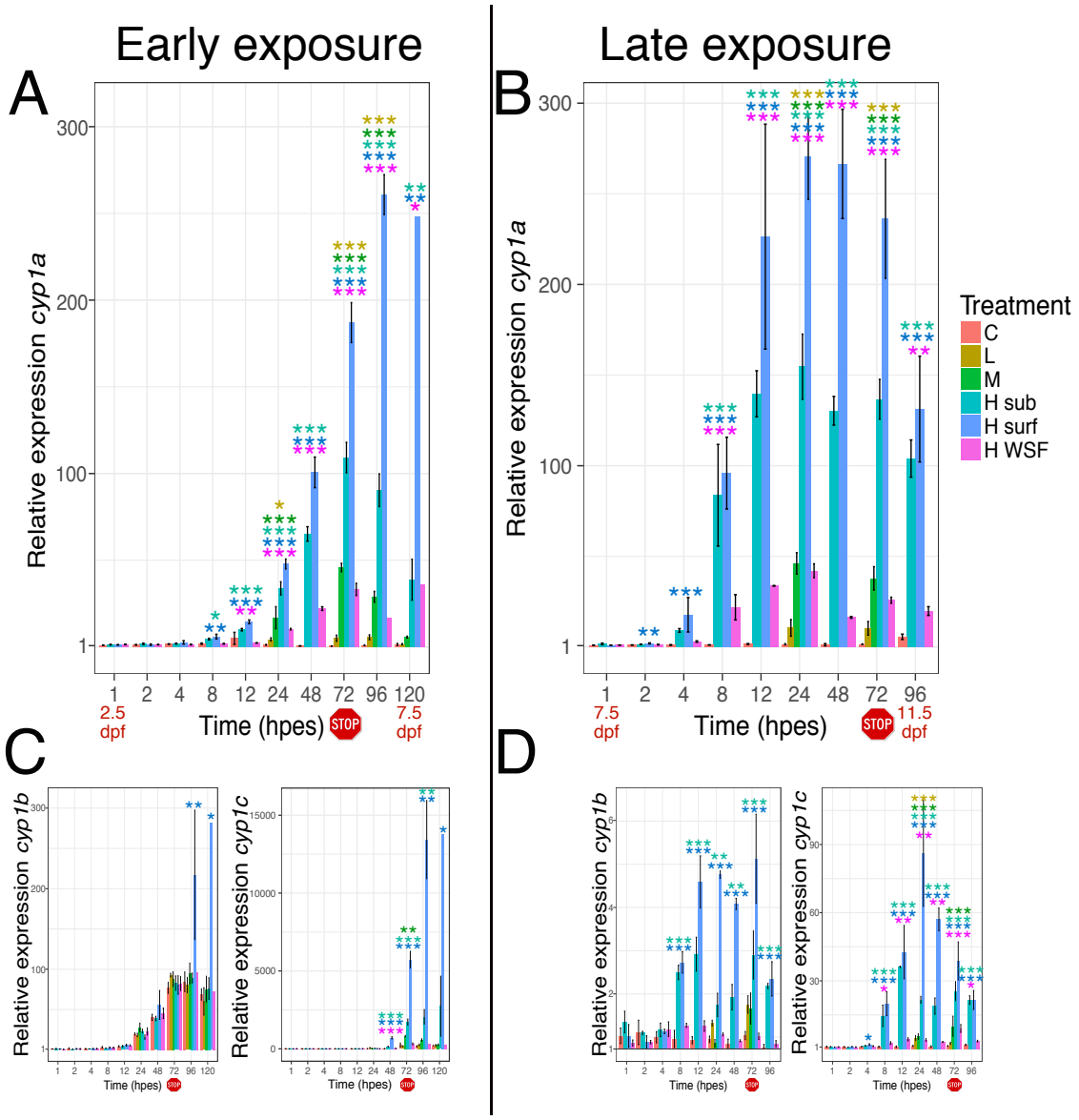

Figure 5: ***Relative expression of cyp1s.*** *Relative expression of cyp1a after early (A) and late (B) exposure. C) shows relative expression of cyp1b (left panel) and cyp1c (right panel) after early exposure, while D) displays cyp1b (Left panel) and cyp1c (right panel) after Late exposure. Expression was related to control group at exposure start to detect both developmental and treatment related expression. Exposure stop is indicated with a stop icon. Statistical difference from control at each time point was tested with One-way ANOVA with Dunnet´s multiple comparsions and significant differences are indicated by *=p<0.05, **=p<0.01 or ***: p<0.001. At 120 hpes in the early exposure, only one sample was collected for H surf and H WSF. Hpes: hours post exposure start, Dpf: days post exposure, C: control, L: low dose, M: medium dose, H sub: high dose submerged, H surf: high dose surface, H WSF: high dose WSF.*

Cyp1a activity

504 Ethoxyresorufin-O-deethylase (EROD) assay was applied to detect Cyp1a activity and
505 was measured at 72 hpes (5.5 dpf) in the *early* exposure. Cyp1a activity was detected in the
506 skin, mainly in the trunk, and in the otoliths in the *H sub* and *H surf* exposures. Low and
507 medium doses showed EROD activity in the trunk, while very little activity was detected in *H*
508 *WSF* (Fig. S9). No specific fluorescence was detected in the embryos incubated in DMSO
509 (images not shown). The internal fluorescence activity of the PAHs in the oil droplets are
510 shown in Figure S9C.
511
512 **Crude oil induced malformations**
513 Craniofacial, eye and growth abnormalities were seen in both exposures (Table 1). We
514 defined six distinct dose-dependent craniofacial phenotypes, given here in increasing severity:
515 mild Bulldog (MBD) and Bulldog (BD) with reduced upper jaw, Upper Jawbreaker (UJB) with
516 a posteriorly twisted upper jaw, Total Jawbreaker (TJB) with posteriorly twisted jaws in
517 general, Darth Vader (DV) with an underdeveloped upper jaw and hanging lower jaw and
518 Hunchback (HB) with severe reduction of all jaw structures with reduced brain structures,
519 abnormal finfold, spinal curvature and poor dorsal rotation of the head (Fig. 6).
520 In the *early* exposure, most severe craniofacial malformations were observed in the *H*
521 *surf* group (Fig. 6A, lower panel Table 1), where all animals were characterized as DVs or HBs
522 (Fig. 6A). The *H sub* group possessed fewer malformations (50%) and the group comprised of
523 BD/MBD, UJB and TJB animals and a few DVs (Fig. 6A, Table 1). In the *H WSF* dose, no
524 malformed phenotypes were observed while low and medium dose both had occasions of the
525 milder phenotypes (MBD/BD and UJB, 28%) (Fig. 6A, Table 1). The abnormal jaw phenotypes
526 were linked to the shorter ethmoid plate. In accordance with the phenotypic observations, both
527 *H sub* and *H surf* groups with the most severe jaw effects also showed a significantly reduced
528 ethmoid plate (14% and 72% shorter, respectively). While the *H WSF*, low dose and medium
529 dose showed no significant reduction in ethmoid plate compared to control (Table 1). Similarly,
530 the total length of the larvae were only significantly reduced in the *H sub* and *H surf* groups
531 (Table 1).
532 In the *late* exposure, the craniofacial malformations were generally milder, and the
533 difference between the *H sub* and *H surf* groups were less evident (Fig. 6). The same phenotypes
534 were present (MBD/BD, TJB and DV) but with an increased proportion in the surface group
535 where all had craniofacial malformations (Fig. 6, Table 1). The *H WSF* group had
536 approximately the same occurrence of the mildest phenotype (MBD/BD, 15 vs 19%) as the low
537 dose (Table 1). In comparison, the medium dose had slightly lower occurrence of the mildest

phenotypes (MBD/BD, 17%) , but additionally had incidents of the more severe phenotypes (TJB and DV, 6%) (Table 1). Along with craniofacial phenotype, the ethmoid plate was significantly reduced in the *H sub* and *H surf* groups (Table 1). Total length of the larvae was reduced in all exposed groups (Table 1).

Eye shape and diameter were affected by oil exposure at both time points. Four eye phenotypes were observed: no phenotype, normal round shape (no), bend shape (be), irregular shape (irr) and protruding lens (pl) (Table 1). The frequency of any eye phenotype was higher in the *early* exposed animals, and the most severe phenotype, protruding lens, was only found in *H sub* (8%) and *H surf* (12%) groups. No effect on eye shape was seen in *H WSF* regardless of timing of exposure (Table 1). Severe reduction in eye diameter was found in the *early* exposed *H surf* and *H sub* animals (Table 1). Less effect on eye size was observed in the *late* exposure, only medium showed significantly reduced eye diameter.

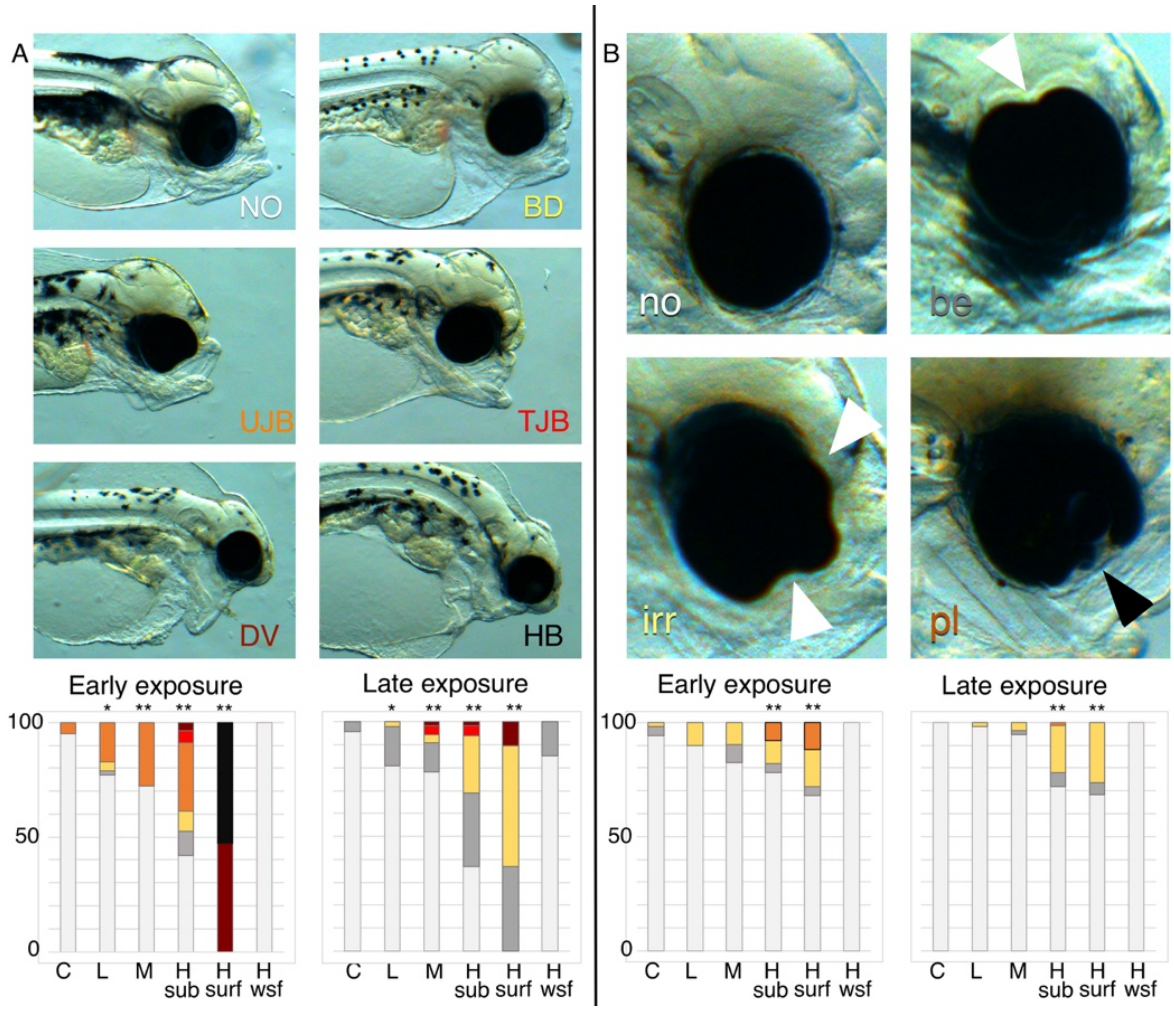

Figure 6: ***Oil induced craniofacial and eye phenotypes.*** *A) Oil induced craniofacial phenotypes, NO: normal, BD: Bulldog, UJB: Upper jawbreaker, TJB: Total jawbreaker, DV: Darth Vader, HB: Hunchback. The bottom panel shows the distribution of the craniofacial phenotypes after early and late exposure at 3 days post hatching. Coloration code: white: NO, grey: mild BD, yellow: BD, orange:*

UJB, red: TJB, dark red: DV, black: HB. B) Oil induced eye phenotypes, no: normal eye shape (white), be: bend shape (grey), irr: irregular shape (yellow), pl: protruding lens (orange). Bottom panel shows the distribution of eye phenotypes in early and late exposures. White arrow heads indicate irregularities in the eye shape, and black arrow head indicate protruding lens.

*Statistical difference from control was tested with Chi-square, and p<0.01 is indicated by **. C: control, L: low dose, M: medium dose, H sub: high dose submerged, H surf: high dose surface, H WSF: high dose water soluble fraction.*

TABLE 1		Total length		Ethmoid plate		Eye diameter		Craniofacial phenotype							Eye phenotype				Cardiac looping			
		Average +/- SD	N	Average	N	Average +/- SD	N	No	MBD	BD	UJB	TJB	DV	HB	no	be	irr	pl	nlo	plo	splo	p value
Early exposure 3 dph	Control	4836 +/- 325	59	170.3 +/- 28,1	51	174,9 +/- 17,4	52	95	0	0	5	0	0	0	94	4	2	0	93	7	0	
	Low dose	4777 +/- 394	47	161,8 +/- 24,1	47	184,3 +/- 12,7	47	77	2	4	17	0	0	0	90	0	9	0	76	24	0	0.0054 **
	Medium dose	4732 +/- 270	61	174,1 +/- 19,4	61	177,2 +/- 12,3	59	72	0	0	28	0	0	0	82	8	10	0	60	40	0	<0.00001 ***
	High submerged	4567 +/- 399***	60	146,6 +/- 19,4***	61	167,4 +/- 15,6***	60	42	11	9	30	5	4	0	78	4	10	8	31	57	11	<0.00001 ***
	High surface	3547 +/- 371***	18	46,6 +/- 37,0***	19	130,9 +/- 8,8***	20	0	0	0	0	0	47	53	68	4	16	12	0	0	100	<0.00001 ***
	High WSF	4769 +/- 269	20	163,7 +/- 24,1	20	186,8 +/- 12,5	20	100	0	0	0	0	0	0	100	0	0	0	95	5	0	0.86
Late exposure 3 dph	Control	4704 +/- 172	75	155,9 +/- 21,2	79	177,2 +/- 9,4	78	96	4	0	0	0	0	0	100	0	0	0	88	12	0	
	Low dose	4589 +/- 193*	59	148,2 +/- 17,0	59	178,6 +/- 8,7	59	81	17	2	0	0	0	0	98	0	2	0	95	5	0	0.24
	Medium dose	4559 +/- 153***	58	154,0 +/- 26,3	59	172,8 +/- 9,9*	58	78	13	4	0	4	2	0	95	2	4	0	74	26	0	0.047 *
	High submerged	4487 +/- 293***	97	123,8 +/- 26,9***	74	173,4 +/- 10,8	78	37	32	25	0	4	1	0	72	6	21	1	42	58	0	<0.00001 ***
	High surface	4320 +/- 175***	20	116,4 +/- 18,6***	20	172,9 +/- 8,9	19	0	37	53	0	0	11	0	68	5	26	0	20	80	0	<0.00001 ***
	High WSF	4532 +/- 179**	20	149,3 +/- 30,2	20	182,6 +/- 7,1	19	85	15	0	0	0	0	0	100	0	0	0	90	10	0	0.91

*Table 1: **Morphological abnormalities after early and late embryonic exposure**. WSF; water soluble fraction, SD; standard deviation, N; total number of animals analyzed, No; normal phenotype, MBD; mild bulldog phenotype, BD; bulldog phenotype, UJB; upper jawbreaker phenotype, TJB; total jawbreaker phenotype, DV; Darth Vader phenotype, HB; hunchback phenotype, no; normal eye shape be; bend eye shape, irr; irregular eye shape, pl; protruding lens, nlo; normal looping, plo; poor looping, splo; severely poor looping. Statistical significant difference from control is indicated by asterisks; p<0.05 *, p<0.001 **. P<0.0001 ***.*

Cardiac malformations

Morphological abnormalities.

The size of the heart was reduced in both exposures, but only *early* exposure resulted in severly malformed hearts with poor looping (Table 2). After *early* exposure, an effect on atrial dimensions was only detected in the *H surf* and *H sub* group (Table 2). The ventricular diastolic diameter was reduced in all exposure groups (9-43%) except for *H WSF*, and the *H surf* group also showed reduced ventricular systolic diameter (38%) (Table 2). There was no effect on atrial dimensions after *late* exposure in any of the doses. However, ventricular systolic and diastolic diameters were reduced in both *H sub* (12% and 19%, respectively) and *H surf* groups (19% and 31%, respectively) in the *late* exposure (Table 2). The hearts were not as malformed as in the *early* exposure, and no incidences of severly poor looping was observed (Table 2).

Functional abnormalities

In both exposures ventricular contractility (VFS) was reduced (Table 2). Notably, reduced contractility was also evident in the lower doses in the *early* exposure. In addition, several animals suffered from a non-contracting or constantly contracting ventricle, defined as silent ventricle (SiV). In the *early* exposure, we observed a dose-dependent prevalence of SiV in all groups with oil droplets, with the most occurrences (73%) in the *H surf* group with the severely abnormally shaped hearts. The only group in *early* exposure with no incidence of SiV was *H WSF* . In the *late* exposure, there were fewer SiVs in all doses, however, we still observed SiV in 60 % of the *H surf* animals, even though their hearts´ morphology looked normal compared to the *early* exposed animals. Reduced heart rate (bradycardia) was only observed in the high surface at the *early* exposure, while increased heart rate (tachycardia) was seen in *H WSF* in the *late* exposure (Table 2).

Edema formation, a consequence of circulation abnormalities, was seen among more treatments in the *late* exposure (Table 2). In the *early* exposure, both *H WSF* (26%) and *H surf* (30%) group had increased frequency of edema compared to the control group (15%). While in the *late* exposure, medium (17%) and all high doses (*H WSF* (23%), *H sub* (23%) and *H surf* (28%)) all showed increased frequency of edema compared to control (12%) (Table 2). Yolk sac size is dependent on hatching time and rate of yolk consumption. We observed an increased average yolk sac size, indicating a decreased yolk utilization in the *H surf* group after *early* exposure. The opposite was observed in the *late* exposure, a decreased yolk sac, thus an increased yolk utilization rate in the *M* and *H WSF* groups (Table 2).

TABLE 2		AS		AD		VS		VD		AFS %		VFS %		Edema		Yolk sac		BPM		SiV %	
		Average +/- SD	N	Average +/- SD	N	Average +/- SD	N	Average +/- SD	N	Average +/- SD	N	Average +/- SD	N	Average +/- SD	N	Average +/- SD	N	Average +/- SD	N	%	N
Early exposure 3 dph	Control	101.4 +/- 14.3	42	121.7 +/- 18.4	42	89.9 +/- 13.8	54	105.8 +/- 19.7	54	17.8 +/-6.9	42	14.4 +/- 6.9	54	15 +/- 8.3	61	21.3 +/- 8.1	61	93.1 +/- 8.7	61	2	54
	Low dose	94.0 +/- 15.3	20	115.4 +/- 18.4	20	85.9 +/- 9.1	34	96.0 +/- 13.3*	34	18.1 +/- 8.2	20	9.8 +/- 6.9*	32	12.3 +/- 6.1	48	24.3 +/- 9.8	48	90.4 +/- 7.4	38	13**	48
	Medium dose	93,5 +/- 13.9	22	113.9 +/- 17.1	22	85.4 +/- 13.5	50	94.1 +/- 15.2**	50	20.2 +/- 8.8	22	8.8 +/- 7.8**	50	13.3 +/- 8.9	61	23.7 +/- 10.7	61	89.2 +/- 9.5	53	24***	51
	High submerged	91.5 +/- 18.2*	42	114.6 +/- 20.2***	44	84.1 +/- 15.6	57	91.7 +/- 19.5***	57	19.8 +/- 8.9	42	7.8 +/- 9.1***	57	17.6 +/- 10.9	61	24.1 +/- 11.2	61	90.5 +/- 10.3	64	20***	40
	High surface	86.2 +/- 14.0**	17	101.0 +/- 18.6	17	56.1 +/- 20.1***	15	59.8 +/- 20.1***	15	13.9 +/- 9.0	17	5.5 +/-12.4***	15	30.0 +/- 13.1***	18	42.5 +/- 11.9***	18	74.9 +/- 15.2***	21	73***	15
	High wsf	99.6 +/- 11.4	15	119.9 +/- 11.7	15	86.1 +/- 8.5	19	105.6 +/- 9.0	19	16.8 +/- 7.0	15	18.4 +/-4.8	19	25.9 +/- 7.1***	20	16.3 +/- 6.6	20	91.7 +/- 5.6	20	0	20
Late exposure 3 dph	Control	98.0 +/- 7.8	50	122.6 +/- 10.8	50	85.7 +/- 16.3	61	102.9 +/- 19.2	61	19.7 +/- 6.3	50	16.2 +/- 6.6	61	12.2 +/- 8.2	79	25.8 +/- 6.8	79	83.2 +/- 7.7	59	2	61
	Low dose	99.3 +/- 10.3	37	122 +/- 13.1	37	83.1 +/- 10.1	49	102.2 +/- 12.9	49	17.8 +/- 8.2	47	17.0 +/- 5.4	47	12.0 +/- 6.8	59	25.1 +/- 5.8	59	82.9 +/- 4.7	77	0	65
	Medium dose	97.6 +/- 12.3	40	120.9 +/- 14.0	40	83.0 +/- 16.0	50	100.2 +/- 19.3	50	18.6 +/- 7.5	40	16.7 +/- 7.9	50	17.2 +/- 9.4**	58	22.1 +/- 8.3**	58	83.4 +/- 5.0	60	4	50
	High submerged	97.9 +/- 9.5	57	121.8 +/- 18.4	57	75.4 +/- 12.3***	69	83.1 +/- 15.3***	69	18.8 +/- 8.0	57	9.9 +/- 7.0***	69	23.4 +/- 11.7***	78	23.5 +/- 6.4	78	82.8 +/- 4.5	78	9*	69
	High surface	97.5 +/- 9.9	19	118.8 +/- 14.6	19	69.6 +/- 7.6***	20	71.3 +/- 9.7***	20	17.5 +/- 7.4	19	2.3 +/- 3.4***	20	28.3 +/- 8.2***	20	21.7 +/- 3.7	20	84.8 +/- 4.8	19	60***	20
	High wsf	99.9 +/- 10.0	18	124.4 +/- 8.9	18	84.1 +/- 9.7	21	102.2 +/- 11.3	21	19.7 +/- 6.2	18	17.6 +/- 5.2	21	23.0 +/- 8.4***	20	16.3 +/- 2.8***	20	90.0 +/- 4.6***	19	0	21

Table 2: ***Cardiac abnormalities after early and late embryonic exposure.*** *WSF; water soluble fraction, AS; atrial systolic diameter, N; Number of animals analyzed, AD; Atrial diastolic diameter, VS; Ventricular systolic diameter, VD; Ventricular diastolic diameter, AFS; Atrial fractional shortening, VFS; ventricular fractional shortening, BPM; Beats per minute, SiV; Silent ventricle. Statistical significant difference from control is indicated by asterisks; p<0.05 *, p<0.001 **. P<0.0001 ***.*

Temporal expression of genes in response to *early* and *late* oil exposure

613 Generally, the response in gene expression was different for each gene between the two
614 exposures (Fig. 7). Oil-induced differential expression of *bmp10* was independent of circulation
615 with an immediate trend of up-regulation in the *late* exposure . While *rhag* and *abcb1* were
616 delayed, with expression increasing after *cyp1a* expression had increased. Expression dynamics
617 for the control group in all genes are shown in Fig. S8.
618 Exposure-related up-regulation of *bmp10,* a calcium regulated gene involved in
619 cardiogenesis, was observed before first heart beat at the cardiac cone stage (72 hpes), 2.4 fold
620 expression in *H surf* compared to control (Fig. 7). The exposure start in the *early* exposure was
621 at the beginning of gastrulation, prior to or at the time of onset of zygotic transcription. Thus,
622 at exposure start no expression of the potent signaling molecule, Bmp10, was detected at the
623 mRNA level. Induction of *bmp10* (~7 fold) was first initiated at 4 dpf (48 hpes) in all groups
624 including control and showed an increasing expression throughout the measured period.
625 Significant up-regulation in the *H surf* group was observed at 72 and 96 hpes in the *early*
626 exposure (Fig. 7A). At the *late* exposure the expression of *bmp10* was more variable throughout
627 the period. A trend of up-regulation was seen from 4 hpes. In particular, *H sub* and *H surf*
628 groups were significantly different from control overall in the investigated period (Two-way
629 ANOVA $p<0.01$) (Fig. 7B). No significant expression changes were detected at 3 dph after
630 either early or late exposure (Fig S7E).
631 Significant up-regulation of the mRNA encoding the transporter protein Abcb1 was
632 seen after *early* exposure but during *late* exposure (Fig. 7). In the *early* exposure, up-regulation
633 was only seen in *H sub* and *H surf* groups (Fig. 7A). While in the late exposure, up-regulation
634 was observed in medium and all high doses (Fig. 7B) . No differential expression of *abcb1* was
635 seen at 3 dph after any exposure treatment (Fig. S7H).
636 Up-regulation of the mRNA encoding the ammonium and carbon dioxide transporter
637 Rhag, was seen in *H sub* and *H surf* groups at both exposures (Fig. 7). In the *early* exposure, an
638 oil induced up-regulation of 3.5 fold (H surf) and 2 fold (H sub) was observed first at 96 hpes.
639 Differential expression of *rhag* was much more immediate in the *late* exposure (after
640 completion of organogenesis), and significant up-regulation was seen in both *H sub* (2-3 fold)
641 and *H surf* (3-4 fold) groups at 24 hpes and throughout the examined period. Additionally, low
642 dose up-regulation at 24 hpes (Fig. 7B). No differential expression of *rhag* was detected at 3
643 dph in either *early* or *late* exposure (Fig. S7G).

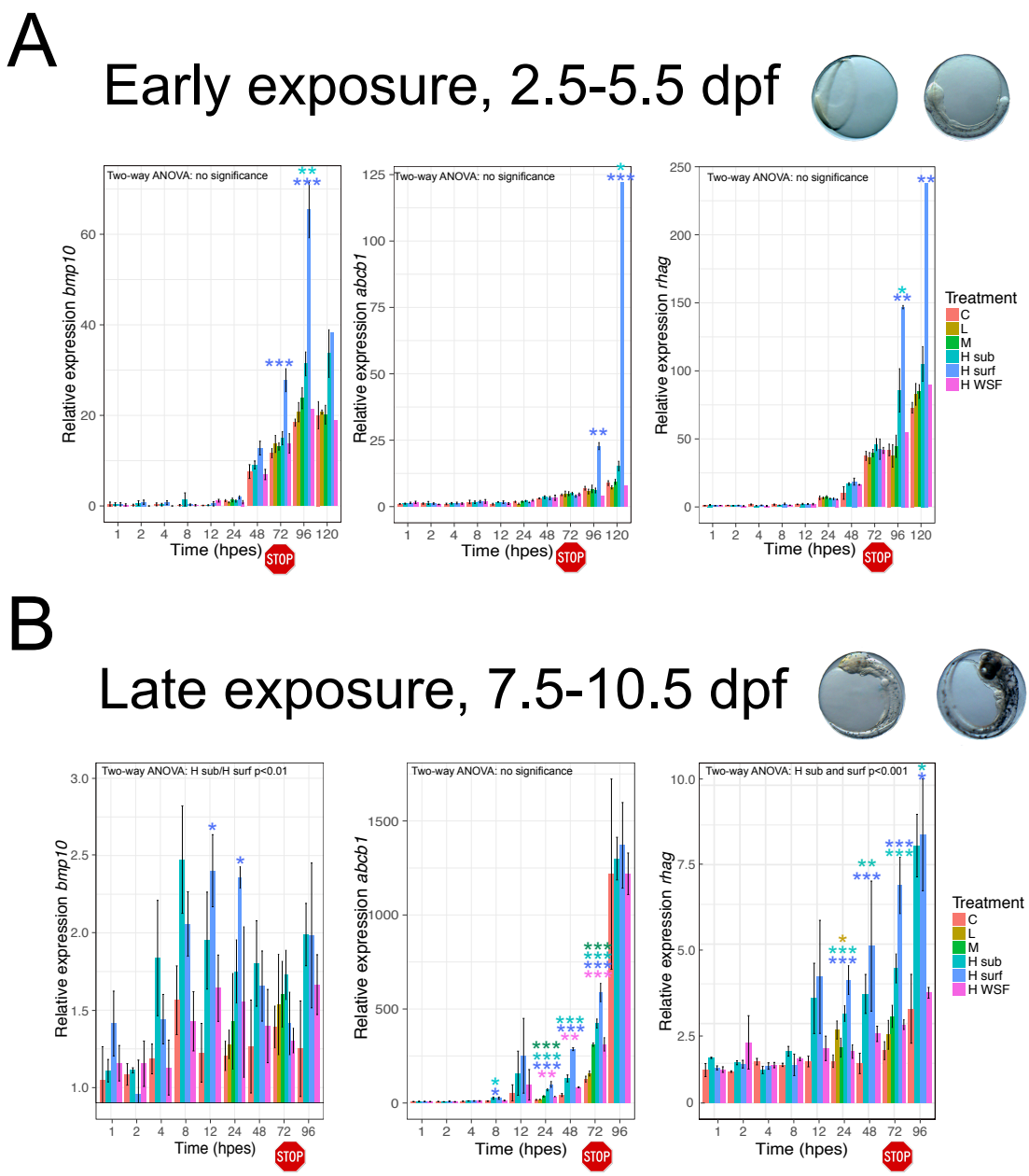

Figure 7: ***Relative expression of bmp10, abcb1 and rhag.*** *Relative expression compared to control at exposure start for bmp10, abcb1 and rhag after early (A) and late (B) exposure. Expression was related to control group at exposure start to detect both developmental and treatment related expression. Exposure stop is indicated by a stop icon. Statistical difference to control was tested at each time point with one-way ANOVA with Dunnet´s multiple comparsions, and significant differences are indicated by *=p<0.05 or ***: p<0.001. At 120 hpes in the early exposure, only one sample was collected for H surf and H WSF.Dpf: days post fertilization, hpes: hours post exposure start, C: control, L: low dose, M: medium dose, H sub: high dose submerged, H surf: high dose surface, H WSF: high dose water soluble fraction.*

Whole mount in situ hybridization of rhag

To determine location of *rhag* in early life stages of fish, we performed whole mount in situ (WISH) on unexposed 10 dpf embryos (Fig. 8). In unexposed 10 dpf Atlantic haddock embryos, expression of *rhag* was observed in a line following the branchial arch blood vessels (Fig. 8). No expression was found anywhere else in the embryos, however, due to auto staining, the yolk sac was removed prior to coloration, and thus, the syncytial layer and yolk sac were not available for analysis. The technical negative control (sense) showed no coloration (Fig. 8C).

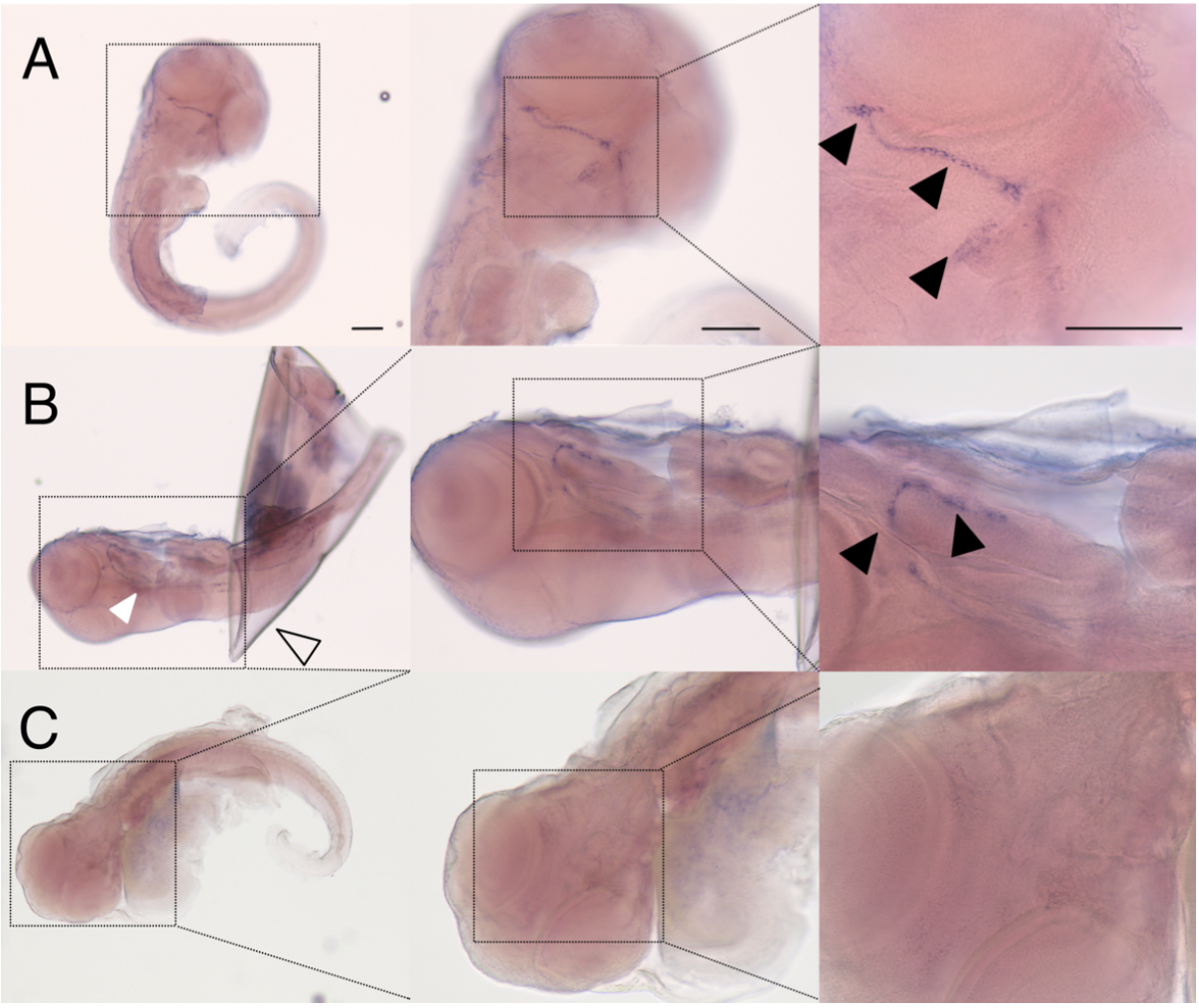

Figure 8. ***Whole mount in situ hybridization of rhag.*** *Expression pattern of rhag in ventral (A) and lateral (B) view in 10 dpf unexposed embryos of Atlantic haddock. Expression is following the branchial arch. C) No labeling in sense control. Black arrow head: expression of rhag, open arrow: eggshell, white arrow head: unspecific coloration of otholites.*

Discussion

671 In this study we aimed to link the consequences of short-term crude oil exposures in
672 two embryonic phases to metabolism and abnormal circulation by investigating morphological
673 and functional phenotypes and related gene expression. In general, the embryotoxic
674 consequences of an oil exposure were more severe in the *early* exposure animals. Severe cardiac
675 and craniofacial abnormalities in the highest doses exposed to micro oil droplets were
676 highlighted. The large difference in phenotypic outcome in *early* vs *late* exposure could be
677 explained both by the prolonged exposure and immature response system. First, particularly in
678 the *early* exposure, the groups exposed to micro oil droplets experienced a prolonged exposure
679 evident by visible oil droplets on the chorion and a prolonged *cyp1a* response. Second, the *early*
680 exposure started prior to or at the time of onset of zygotic transcription, in which the embryo
681 has a less efficient response and detoxification system (Sørhus et al., 2016a). Consequently, we
682 observed a delayed response in gene expression of all genes evaluated, including *cyp1a* which
683 is crucial for the first phase in xenobiotic metabolism (Goksøyr, 1995). Higher oil droplet
684 binding and most likely, accumulation, contributed to a higher body burden of PAHs in the
685 *early* exposure, while the levels of PHE metabolites were 2-3 times higher in the *late* exposure.
686 These results are in line with studies showing that Cyp1a induction has a protective rather than
687 aggravating effect (Incardona et al., 2005; Wells et al., 1997; Wells et al., 2009).
688 Exposing embryos at two developmental time points gave us a unique opportunity to
689 phenotypically anchor temporal gene expression changes and continue to unravel underlying
690 mechanisms of crude oil toxicity. Exposure during early cardiac development, and after onset
691 of heartbeat enabled us to evaluate whether the expression response for the various genes were
692 due to direct effect or secondary to abnormal circulation. Furthermore, we linked gene
693 expression to metabolism by investigating expression in context of Cyp1a regulation, PAH
694 uptake and appearance of metabolites. Mainly, we suggest that *cyp1a*, *cyp1b*, *cyp1c* and *bmp10*
695 are directly induced by parent compounds in the oil. To illustrate, these genes are expressed in
696 the *late* exposure before metabolites are detected. Subsequently, *abcb1* and *rhag,* which are
697 linked to transport of xenobiotic products (Choudhuri and Klaassen, 2006) and nitrogenous
698 waste (Caner et al., 2015), respectively, showed a delayed response corresponding to xenobiotic
699 energy consumption utilizing amino acids (Wang et al., 2019) and transport in xenobiotic
700 metabolism (Kimura et al., 2007).
701
702 **Oil droplet fouling**
703 Oil droplet fouling occured in both *H surf* and *H sub* groups and consequently increased
704 haddock embryotoxicity by escalating the uptake and prolonging the exposure. Droplet fouling

705 on the submerged exposures show that accumulation of oil droplets was due to the biological
706 characteristics of the haddock embryo and not a surface slick artifact. Unlike other cod fish
707 eggs, haddock have an extra membrane of adhesive material covering the primary egg envelope
708 (Hansen et al., 2018; Morrison et al., 1999; Oppen-Berntsen et al., 1990). The chemical
709 composition of this outer membrane is still unknown. However, it clearly has a hydrophopic
710 interaction with oil, and it is responsible for the accumulation of oil droplets on the eggshell.
711 The outer membrane degrades during the embryo phase, a few days before hatching (Sørhus et
712 al., 2015, 2016). Accordingly, the early egg stages accumulated more oil droplets than the late
713 stages in the present study.

714 Haddock spawn at depths between 30 and 500 meters (Olsen et al., 2010; Solemdal et
715 al., 1997). The eggs have a natural high buoyancy, and all embryonic stages have been observed
716 in the surface at surveillances (Solemdal et al., 1997). Oil droplet fouling can increase the
717 buoyancy of the egg, both by the low density of oil itself, but also by trapping of air bubbles on
718 the chorion (Sørhus et al., 2015). In contrast, we have also observed that haddock eggs with oil
719 droplets become negatively buoyant just before hatching and then sink to the bottom of the
720 exposure tanks. Similar effects have been observed in oil-exposed mahi mahi (*Coryphaena*
721 *hippurus*) (Pasparakis et al., 2017). The mechanism behind this remains unclear, but one
722 possibility is loss of water due to disruption of the perivetiline membrane or disruption of the
723 osmotic control (Pasparakis et al., 2017). Even though we did observe some slick formation as
724 seen in the *H surf* group, we argue that this group is also the more ecologically relevant exposure
725 dose. In a situation where crude oil is discharged at depths like in the Deepwater Horizon
726 accident or in a rough sea, oil droplets will be located throughout the water column (Hansen et
727 al., 2019; Nordtug et al., 2011). Consequently, oil droplet fouling increases buoyancy, that will
728 lead to increased speed to the surface and to even greater exposures in the oil slick.

729 Oil droplet fouling most likely causes transfer of more and higher molecular weight oil
730 components to the embryo. Although the nominal oil water dose in *H WSF* were higher than *M*
731 sub group, both PAH uptake and *cyp1a* induction were mainly higher in *M* sub group compared
732 to *H WSF* group especially in the *early* exposure. Interestingly, the composition of PAHs was
733 also different. Nearly no high molecular weight (5-6-rings) PAHs were found in the PAH tissue
734 of the *H WSF* group in any exposure. Accordingly, the *H WSF* group had very little Cyp1a
735 activity (EROD assay) compared to all other treatments where oil droplets were included.

736 In haddock embryos, oil droplets possibly add a dual toxicity. First, oil droplet fouling
737 results in an increased local concentration of PAHs and other toxic oil components. Second, oil
738 droplets adhered to the chorion may also contribute to transfer of lipophilic compounds that are

739 less available in a general water exposure (Sørensen et al., 2017). The latter may be linked to
740 the high molecular weight PAHs which were not present in the *H WSF.* Enhanced toxicity after
741 direct contact with oil and accumulation on the chorion have also been observed in medaka
742 (*Oryzias latipes*) (Gonzalez-Doncel et al., 2008) and polar cod (Laurel et al., 2019), together
743 with our results it highlight the importance of including dispersed oil in experimental exposure
744 designs and risk assessment models (Nordtug et al., 2011).
745
746 **PAH uptake, Cyp induction and metabolism**
747 We observed an immature detoxification system in early embryos via delayed
748 expression of *cyp1* paralogs and *abcb1* transporter, higher body burdens of PAHs and lower
749 levels of metabolites. Xenobiotic metabolism is necessary to excrete toxic substances. Among
750 the thousands of potential PAH metabolites, we used PHE as a model compound to study the
751 metabolic capacity of the haddock embryo. Even though PHE is a weak inducer of *cyp1s,* we
752 report PHE metabolite levels as to represent metabolite formation of any kind. The *late*
753 exposure had the more efficient elimination of PAHs evidenced by the immediate strong *cyp1*
754 response resulting in lower peak levels of tissue PAHs and higher levels of metabolites (e.g.
755 PAH levels were approximately 2.5 times lower in *H surf late* compared to *early* exposure). In
756 the *late* exposure *cyp1a, cyp1b* and *cyp1c* mRNA was highly and quickly induced, and already
757 after 24 hours the metabolic capacity surpassed the uptake speed of PHE. This resulted in a
758 reduced body burden even under continuous exposure. However, we did not observe any high
759 accumulation of PHE metabolites, showing that the embryos can effeciently excrete metabolic
760 products during phase III metabolism.
761 Cyp1a mRNA was clearly the first and the main detoxification enzyme mRNA in *early*
762 embryonic development. The other *cyp1* paralogs, *cyp1b* and *cyp1c,* were not induced until later
763 in the *early* exposure. *cyp1b* was upregulated from 3.5 dpf (24 hpes) regardless of exposure
764 including control and emphasizes the other non-detoxifying roles of Cyp1s (e.g. steroid
765 biosynthesis and cardiovascular and eye development (Chaudhary et al., 2009; Li et al., 2017))
766 during early fish development (Goldstone et al., 2010). At 72 hpes a 200 fold developmentally
767 related up-regulation of *cyp1c* was observed and at the same time a strong up-regulation was
768 seen in the treatment groups. These observations suggests that xenobiotic induction of *cyp1c* is
769 occurring as soon as the organism possess Cyp1c acitivity. A delayed expression of *cyp1b* and
770 *cyp1c* underscore the differences in capability for fish embryos to metabolize xenobiotics
771 depending on their embryonic developmental window. Our results coincide with the findings

772 of (Kuhnert et al., 2017) where the expression of *cyp1b* and *cyp1c* is also delayed in zebrafish
773 exposed to benzo(a)pyrene.
774 While Cyp1a appears protective and is necessary for detoxification (Billiard et al., 2006;
775 Mu et al., 2016; Scott et al., 2011; Wincent et al., 2015), it may also result in the production of
776 some reactive toxic metabolites (Wells et al., 1997). Other enzymes can also produce
777 metabolites that can increase the toxicity (Nebert et al., 2004). Several studies have found that
778 hydroxylated PAHs have greater toxic effects than the parent compounds (Chibwe et al., 2015;
779 Diamante et al., 2017; Fallahtafti et al., 2012; Schrlau et al., 2017). Bioactivation of PAHs has
780 also been linked to endocrine disruption (Fernandes and Porte, 2013; Hyzd'alova et al., 2018;
781 Pencikova et al., 2019; Sievers et al., 2013; Van de Wiele et al., 2005). Moreover, electrophilic
782 intermediates of PAH metabolism are well known for the formation of hydrophobic DNA
783 adducts and cancer induction (Moorthy et al., 2015). PAH metabolites may also play an
784 important role in cardiotoxicity. PHE and oil are shown to block currents of K^+ through the
785 ERG potassium channel (Brette et al., 2014; Brette et al., 2017). However, the exact mechanism
786 behind how three-ring PAHs are able to block the channel is not well defined (Incardona, 2017).
787 *In silico* docking models suggest that PHE has the necessary three aromatic rings, but lacks any
788 other functional groups essential for strong blocking capacity (Cavalli et al., 2012; Vandenberg
789 et al., 2012). Other types of membrane ion channels have been intensively studied through the
790 use of PAH metabolites: The 9-hydroxy-PHE metabolite (9-phenanthrol) is a selective and
791 sensitive blocker of the transient receptor potential melastatin 4 channels (TRPM4) (Burris et
792 al., 2015; Guinamard et al., 2014; Hou et al., 2018) and anthracene-9-carboxylic acid is a
793 commonly used blocker of the calcium-activated chloride channels (CaCCs) (TMEM16A)
794 channels (Cherian et al., 2015; Ta et al., 2016). The blocking capacity of PAH metabolites to
795 the ERG channels has not yet been studied to our knowledge, but it is possible, if not likely,
796 that critical aspects of crude oil cardiotoxicity are caused by an ERG-blocking PAH metabolite.
797 Taken together we see a need for more studies of the effects of PAH metabolism in oil toxicity,
798 and urge more labs to develope analytical methods able to cover a broad spectra of oil-related
799 metabolites. The latter is a great methological challenge due to extreme complexeity in the
800 number of metabolites and the lack of available standards.
801 We show that *cyp1* mRNA induction, PAH tissue content, and PAH metabolites are
802 related to early life stage toxicity in fish, where the amount of mRNA induction and PAH and
803 metabolite levels is related to the window of exposure. This observation is in line with an
804 established relationship between toxicity and PAHs in crude oil (Carls and Meador, 2009;
805 Hodson, 2017) and petrogenic substances (Adams et al., 2014; Kamelia et al., 2019; Kamelia

806 et al., 2017). However, there are multiple toxic components in crude oil apart from PAHs that
807 can induce toxicity in early life stages of fish (Meador and Nahrgang, 2019; Sorensen et al.,
808 2019). Therefore, there is a need for more fractionation studies and Effect Directed Analysis
809 (EDA) to increase our understanding of the additive and synergetic effects of the complex oil
810 toxicity.
811
812 **Morphological abnormalities**
813 The large differences in morphological abnormalities after *early* vs *late* exposure~~,~~ show
814 the importance of timing of exposure. The *early* exposure has major consequences for
815 formation of organs by interfering with the developmental signaling pathways, while *late*
816 exposure mainly shows effect on organism condition possibly downstream of cardiofunctional
817 defects.
818 The eye abnormalities were most likely downstream of both circulation defects and
819 altered cyp-balance. Crude oil-induced eye developmental defects are well documented. Both
820 reduced eye size (anapthalmia) and reduced size with abnormalities (microphtalmia) are
821 observed (Incardona, 2014; Lie et al., 2019; Magnuson et al., 2018). In the present study, eye
822 size was mainly affected in the *early* exposure, where we find the most severe developmental
823 and functional abnormalities. Zebrafish with no cardiac function (*tnnt* morpholinos) mimic the
824 oil-induced reduction in eye size (Incardona et al., 2004), suggesting that anapthalmia is
825 secondary to circulatory defects. However, it is also suggested that abnormal cyp-balance
826 disrupts retinoic acid signaling pathway through disturbance of Cyp26, leading to abnormal eye
827 development (Lie et al., 2019; Yamamoto et al., 2000). Another Cyp enzyme, Cyp1b, is also
828 involved in eye development (regulating ocular fissure closure) through both retinoic acid-
829 dependent and -independent pathways (Chambers et al., 2007; Williams et al., 2017).
830 Affirmative of a non-toxicological function of Cyp1b was the general increase in expression of
831 *cyp1b* beginning at 3.5 dpf (24 hpes). Overexpression of *cyp1b* causes irregular eye shape
832 referred to as coloboma (Chambers et al., 2007; Williams et al., 2017). The *late* exposure
833 animals possessed less severe abnormalities in general. However, the *H sub* and *H surf* groups
834 still showed excessive incidence of eye abnormalities (irregular eye shape) which were
835 reflected in increased *cyp1b* expression. These findings are in line with findings that proper
836 closure of the ocular fissure is disrupted by overexpression of *cyp1b* (Chambers et al., 2007;
837 Williams et al., 2017).
838 The craniofacial abnormalities observed in our exposed animals are potentially due to
839 both disruption of jaw and pharyngeal arch formation and reduced outgrowth linked to

840 abnormal craniofacial muscle function. Expression of Cyp1b was found in pharyngeal arches
841 of zebrafish exposed to PCB 126 and TCDD (Timme-Laragy et al., 2008; Yin et al., 2008), and
842 the injection of human *cyp1b* mRNA resulted in disruption of neural crest-derived jaw and
843 pharyngeal arch formation (Williams et al., 2017). Furthermore, muscle contraction is
844 mandatory for proper stacking of chondrocytes and outgrowth of craniofacial cartilages
845 (Shwartz et al., 2012). Crude oil disrupts cardiac muscle function (Brette et al., 2014; Brette et
846 al., 2017; Incardona, 2014), and jaw spasms observed in previous studies suggest a similar
847 effect on the craniofacial muscles. Impairment of craniofacial muscles might explain the high
848 incidences of craniofacial abnormalites in the *late* exposure. In conclusion, the tight correlation
849 between *cyp1b* expression and oil induced eye and jaw deformities suggests that inappropriate
850 expression of *cyp1b* in oil-exposed animals are directly linked to abnormal eye and jaw
851 development.
852
853 **Cardiac morphological defects**
854 The severely malformed and small hearts after *early* exposure imply multiple impacts
855 on cardiac formation and early development, while the reduced heart size after *late* exposure
856 suggests on late development and especially cardiomyocyte proliferation.
857 A circulation- and time-independent expression of *bmp10* suggests a direct effect of
858 crude oil on calcium homeostasis. Several signaling pathways linked to cardiac development
859 and proliferation are impacted by the complexity of crude oil exposure, including calcium-
860 regulated pathways (Sørhus et al., 2017; Xu et al., 2017), AhR (Yin et al., 2008) and retinoic
861 acid (Lie et al., 2019)- dependent pathways. Disruption of intracellular calcium levels has been
862 shown to reduce cardiomyocyte proliferation leading to smaller ventricles (Ebert et al., 2005;
863 Rottbauer et al., 2001), suggesting that ventricular proliferation is calcium controlled. Bmp10
864 is a calcium-regulated signaling molecule involved in cardiogenesis (Huang et al., 2012;
865 Wamhoff et al., 2004; Wamhoff et al., 2006) and is thought to orchestrate several major key
866 cardiogenic factors and play a part in ventricular cell proliferation (Chen et al., 2004; Shou et
867 al., 1998). In the current study, we observed an up-regulation of *bmp10* regardless of timing of
868 exposure. However, the developmental consequences of timing of an inapropriate gene
869 regulation is essential. In the *early* exposure, the initiation of *bmp10* up-regulation was
870 occurring at cardiac cone stage (72 hpes). At this developmental time point asymmetric Bmp
871 signaling (in particular bmp4) in the cardiac primordium is involved in the looping of the heart
872 (Chocron et al., 2007; Huang et al., 2012; Lombardo et al., 2019). An overexpression of *bmp10*
873 in the cardiac primordium may therefore disrupt left/right looping of the heart. At the start of

874 the *late* exposure, the looping process was already initiated, and the heart was functionally
875 beating. Consequently, we observed less severe effect on looping, while growth of the heart
876 was altered. Reduced size of the ventricle was observed in both *H sub* and *H surf*, as well as an
877 overall up-regulation of *bmp10*. The up-regulation of *bmp10* may be consequential for the
878 reduced ventricle size in exposed larvae from the late embryonic stages. Taken together, the
879 observations from *early* and *late* exposures support that the oil components have a circulation-
880 independent direct effect on calcium homeostasis likely disrupting cardiac development and
881 proliferation indicated by the up-regulation of *bmp10*.
882
883 **Cardiac functional defects**
884 The cardiac functional defects post-exposure were linked to irreversible
885 morphological changes and reversible effects of circulating crude oil components. Reduced
886 contractility and non-contracting or constantly contracting ventricles (SiV phenotype) were
887 traits found in both *early* and *late* exposures. Functional defects in the *early* exposure could
888 originate from irreversible morphological changes (severly malformed ventricles) but could
889 also stem from consumption of oil components stored in the yolk sac after hatching as
890 observed in previous studies (Sørhus et al., 2016b; Vanleeuwen et al., 1985).. The *late*
891 exposure animals, on the other hand, had normally shaped but often smaller ventricles. The
892 contractility abnormalities most likely stem from components stored in the yolk sac.
893 A suite of defects downstream of cardiac dysfunction has been described for oil-exposed
894 developing fish, including edema accumulation (Incardona, 2017; Incardona and Scholz, 2016).
895 Edema formation measured included both pericardial and yolk sac edemas, and may be due to
896 i) irreversible morphological cardiac deformities that alter the cardiac function later in life and
897 ii) oil components that can directly alter the electrophysiological activity (contractility and
898 rhythm) of the developing heart (Brette et al., 2014; Brette et al., 2017; Incardona, 2017).
899 Circulatory defects may also affect distribution of lipids from the yolk which in turn may affect
900 growth in later stages. Polar cod exposed to transient low levels of oil induced dysregulation of
901 lipid metabolism and reduced growth in morphologically normal juveniles (Laurel et al., 2019).
902 We observed a reduced yolk utilization in *H surf* in the *early* exposure, suggesting that these
903 embryos were deprived of essential yolk-based lipids. Furthermore, the reduced yolk utilization
904 seems to be associated with heart rate, and thus, dependent on circulation. Accordingly, the
905 treatment group~~s~~ with tachycardia had highly increased yolk utilization (*H WSF*), while the
906 treatement group~~s~~ with bradycardia (*H surf*) had severely reduced yolk utilization. Overall,

907 cardiocirculatory defects during embryonic development could be sufficient to impact growth
908 and could be consequential for individual fitness at juvenile and adult stages.
909
910 **Osmoregulation**
911 Up-regulation of *rhag* suggests that osmoregulatory cells are impacted by oil exposure.
912 Osmoregulation can be disrupted by circulatory defects (Miyanishi et al., 2013), or directly
913 affected by oil components (Sørhus et al., 2017). In adult fish, the main localization for
914 osmoregulation, gas exchange and transport of ammonium are in the gills (Evans et al., 2005)
915 in osmoregulatory cells called mitochondrial rich cells (MRCs) (Evans et al., 2005; Hiroi et al.,
916 2005; Hirose et al., 2003; Shelbourne, 1957). In 10 dpf haddock, expression of *rhag* was found
917 in the branchial arches (primordial gills), in close proximity to expected localization of MRCs
918 (Zimmer et al., 2014; Zimmer et al., 2017). This finding coincides with expression of *rhag* in
919 mahi mahi at approximately the same developmental time point (Wang et al., 2019). In both
920 *early* and *late* exposures, *rhag* seemed to track more with the peak of *cyp1a* induction and
921 *abcb1* transporter. This could indicate that energy for Cyp1a-mediated PAH metabolism is
922 derived from amino acids (Pasparakis et al., 2016), generating nitrogenous waste also suggested
923 by Wang et al. (2019). Thus, this increased amount of ammonium waste can also affect
924 osmoregulation capacity of MRCs and consequently lead to increased edema formation.
925 Additionally, ammonia excess in itself can add to the toxicity. In mouse, ammonium perturbs
926 glial cells ability to remove potassium and are therefore toxic to the brain (Thrane et al., 2013).
927 Consequently, the crude oil exposed embryos could experience an internal synergy between
928 internal ammonium toxicity and PAH toxicity.
929
930 **Conclusion**
931 In this study we showed that oil droplet fouling occurred throughout the whole water
932 column and contributed to increased PAH uptake and embryotoxicity. Oil droplet fouling
933 makes the haddock embryo extremely vulnerable to even short, low level oil exposures. The
934 high bioaccumulation of PAHs and lower levels of metabolites in the *early* exposure reflects
935 an immature response system that possibly has an exacerbating toxic effect in early embryos.
936 Short term exposures prior to and after onset of heart beat and frequent sampling regime enabled
937 us to establish direct and downstream effects of crude oil exposure. The relatively rapid and
938 circulatory-independent response in *bmp10* regulation suggested direct effects on calcium
939 homeostasis affecting calcium-regulated developmental pathways, including cardiogenesis.
940 Similarly, we propose that abnormal regulation of *cyp1b* due to oil exposure may affect eye and

941 jaw development. Expression of *rhag* indicates a direct oil effect on osmoregulatory cells and
942 osmoregulation. We recognize that oil is a complex mixture of many potential toxic
943 components. Yet, the strong correlations among PAH uptake, *cyp1a* induction, metabolite
944 formation and malformations suggest that PAH tissue body burden remains a good metric for
945 oil toxicity.

946 Our findings are adding more knowledge about development stage-dependent effects of
947 crude oil exposure. Thus, we provide more knowledge and detail to several existing adverse
948 outcome pathways of crude oil toxicity.

949

950 **Acknowledgements**

951 We would like to acknowledge Stig Ove Utskot and Tobias Hukset for breeding and
952 management of the fish, Charlotte Nakken for technical assistance with the metabolite data,
953 Prescilla Perrichon for discussion of the data and review of the manuscript and Karen Peck for
954 a thorough review of the manuscript. This work was financed by the Research Council of
955 Norway (EGGTOX: Unraveling the mechanistic effects of crude oil toxicity during early life
956 stages of cold-water marine teleosts (Project # 267820), www.forskningsradet.no) and the
957 Institute of Marine Research, Norway. The funders had no role in study design, data collection
958 and analysis, decision to publish, or preparation of the manuscript.

959

960 **Author contributions**

961 Conceived and designed the experiments: E.S., S.M., Ø.K. and A.T.
962 Performed the experiments: E.S., S.M., Ø.K.
963 Analysed and interpreted the data: E.S., S.M., C.E.D., D.D.S.
964 Contributed reagents/materials/analysis tools: A.T., D.D.S.
965 Contributed to the writing of the manuscript: E.S., S.M., C.E.D.
966

967 **Competing interests**

968 The authors declare no competing financial interests.
969

970

971 **References**

972

973 Abramyan, J., 2019. Hedgehog Signaling and Embryonic Craniofacial Disorders. J Dev Biol 7.
974 Adams, J., Bornstein, J.M., Munno, K., Hollebone, B., King, T., Brown, R.S., Hodson, P.V.,
975 2014. Identification of compounds in heavy fuel oil that are chronically toxic to rainbow trout
976 embryos by effects-driven chemical fractionation. Environmental Toxicology and Chemistry
977 33, 825-835.

Andres-Delgado, L., Mercader, N., 2016. Interplay between cardiac function and heart development. Bba-Mol Cell Res 1863, 1707-1716.
Beyer, J., Jonsson, G., Porte, C., Krahn, M.M., Ariese, F., 2010. Analytical methods for determining metabolites of polycyclic aromatic hydrocarbon (PAH) pollutants in fish bile: A review. Environ Toxicol Pharmacol 30, 224-244.
Billiard, S.M., Timme-Laragy, A.R., Wassenberg, D.M., Cockman, C., Di Giulio, R.T., 2006. The role of the aryl hydrocarbon receptor pathway in mediating synergistic developmental toxicity of polycyclic aromatic hydrocarbons to zebrafish. Toxicological sciences : an official journal of the Society of Toxicology 92, 526-536.
Brette, F., Machado, B., Cros, C., Incardona, J.P., Scholz, N.L., Block, B.A., 2014. Crude oil impairs cardiac excitation-contraction coupling in fish. Science 343, 772-776.
Brette, F., Shiels, H.A., Galli, G.L., Cros, C., Incardona, J.P., Scholz, N.L., Block, B.A., 2017. A Novel Cardiotoxic Mechanism for a Pervasive Global Pollutant. Sci. Rep. 7, 41476.
Burris, S.K., Wang, Q., Bulley, S., Neeb, Z.P., Jaggar, J.H., 2015. 9-Phenanthrol inhibits recombinant and arterial myocyte TMEM16A channels. Br J Pharmacol 172, 2459-2468.
Caner, T., Abdulnour-Nakhoul, S., Brown, K., Islam, M.T., Hamm, L.L., Nakhoul, N.L., 2015. Mechanisms of ammonia and ammonium transport by rhesus-associated glycoproteins. Am J Physiol-Cell Ph 309, C747-C758.
Carls, M.G., Meador, J.P., 2009. A perspective on the toxicity of petrogenic PAHs to developing fish embryos related to environmental chemistry. Hum Ecol Risk Assess 15, 1084-1098.
Carroll, J., Vikebo, F., Howell, D., Broch, O.J., Nepstad, R., Augustine, S., Skeie, G.M., Bast, R., Juselius, J., 2018. Assessing impacts of simulated oil spills on the Northeast Arctic cod fishery. Mar. Pollut. Bull. 126, 63-73.
Cavalli, A., Buonfiglio, R., Ianni, C., Masetti, M., Ceccarini, L., Caves, R., Chang, M.W., Mitcheson, J.S., Roberti, M., Recanatini, M., 2012. Computational design and discovery of "minimally structured" hERG blockers. J Med Chem 55, 4010-4014.
Chambers, D., Wilson, L., Maden, M., Lumsden, A., 2007. RALDH-independent generation of retinoic acid during vertebrate embryogenesis by CYP1B1. Development 134, 1369-1383.
Chaudhary, K.R., Batchu, N., Seubert, J.M., 2009. Cytochrome P450 Enzymes and the Heart. Iubmb Life 61, 954-960.
Chen, H.Y., Shi, S., Acosta, L., Li, W.M., Lu, J., Bao, S.D., Chen, Z.A., Yang, Z.C., Schneider, M.D., Chien, K.R., Conway, S.J., Yoder, M.C., Haneline, L.S., Franco, D., Shou, W.N., 2004. BMP10 is essential for maintaining cardiac growth during murine cardiogenesis. Development 131, 2219-2231.
Cherian, O.L., Menini, A., Boccaccio, A., 2015. Multiple effects of anthracene-9-carboxylic acid on the TMEM16B/anoctamin2 calcium-activated chloride channel. Biochim Biophys Acta 1848, 1005-1013.
Chibwe, L., Geier, M.C., Nakamura, J., Tanguay, R.L., Aitken, M.D., Simonich, S.L., 2015. Aerobic Bioremediation of PAH Contaminated Soil Results in Increased Genotoxicity and Developmental Toxicity. Environ. Sci. Technol. 49, 13889-13898.
Chocron, S., Verhoeven, M.C., Rentzsch, F., Hammerschmidt, M., Bakkers, J., 2007. Zebrafish Bmp4 regulates left-right asymmetry at two distinct developmental time points. Dev. Biol. 305, 577-588.
Choudhuri, S., Klaassen, C.D., 2006. Structure, function, expression, genomic organization, and single nucleotide polymorphisms of human ABCB1 (MDR1), ABCC (MRP), and ABCG2 (BCRP) efflux transporters. Int J Toxicol 25, 231-259.
Delling, M., DeCaen, P.G., Doerner, J.F., Febvay, S., Clapham, D.E., 2013. Primary cilia are specialized calcium signalling organelles. Nature 504, 311-314.

1027 Diamante, G., do Amaral, E.S.M.G., Menjivar-Cervantes, N., Xu, E.G., Volz, D.C., Dias Bainy,
1028 A.C., Schlenk, D., 2017. Developmental toxicity of hydroxylated chrysene metabolites in
1029 zebrafish embryos. Aquatic toxicology (Amsterdam, Netherlands) 189, 77-86.
1030 Ebert, A.M., Hume, G.L., Warren, K.S., Cook, N.P., Burns, C.G., Mohideen, M.A., Siegal, G.,
1031 Yelon, D., Fishman, M.C., Garrity, D.M., 2005. Calcium extrusion is critical for cardiac
1032 morphogenesis and rhythm in embryonic zebrafish hearts. P Natl Acad Sci USA 102, 17705-
1033 17710.
1034 Edmunds, R.C., McIntyre, J.K., Luckenbach, J.A., Baldwin, D.H., Incardona, J.P., 2014.
1035 Toward enhanced MIQE compliance: reference residual normalization of qPCR gene
1036 expression data. Journal of Biomolecular Techniques 25, 54-60.
1037 Evans, D.H., Piermarini, P.M., Choe, K.P., 2005. The multifunctional fish gill: Dominant site
1038 of gas exchange, osmoregulation, acid-base regulation, and excretion of nitrogenous waste.
1039 Physiol. Rev. 85, 97-177.
1040 Fallahtafti, S., Rantanen, T., Brown, R.S., Snieckus, V., Hodson, P.V., 2012. Toxicity of
1041 hydroxylated alkyl-phenanthrenes to the early life stages of Japanese medaka (*Oryzias latipes*).
1042 Aquat. toxicol. 106-107, 56-64.
1043 Fernandes, D., Porte, C., 2013. Hydroxylated PAHs alter the synthesis of androgens and
1044 estrogens in subcellular fractions of carp gonads. The Science of the total environment 447,
1045 152-159.
1046 Fridgeirsson, E., 1978. Embryonic development of five species of gadoid fishes in Icelandic
1047 waters. Rit Fiskeideildar 5, 1-68.
1048 Goksøyr, A., 1995. Use of cytochrome P450 1A (CYP1A) in fish as a biomarker of aquatic
1049 pollution. Archives of toxicology. Supplement. = Archiv fur Toxikologie. Supplement 17, 80-
1050 95.
1051 Goksoyr, A., Andersson, T., Hansson, T., Klungsoyr, J., Zhang, Y., Forlin, L., 1987. Species
1052 characteristics of the hepatic xenobiotic and steroid biotransformation systems of two teleost
1053 fish, Atlantic cod (Gadus morhua) and rainbow trout (Salmo gairdneri). Toxicology and applied
1054 pharmacology 89, 347-360.
1055 Goldstone, J.V., McArthur, A.G., Kubota, A., Zanette, J., Parente, T., Jonsson, M.E., Nelson,
1056 D.R., Stegeman, J.J., 2010. Identification and developmental expression of the full complement
1057 of Cytochrome P450 genes in Zebrafish. BMC genomics 11, 643.
1058 Gonzalez-Doncel, M., Gonzalez, L., Fernandez-Torija, C., Navas, J.M., Tarazona, J.V., 2008.
1059 Toxic effects of an oil spill on fish early life stages may not be exclusively associated to PAHs:
1060 studies with Prestige oil and medaka (*Oryzias latipes*). Aquat. toxicol. 87, 280-288.
1061 Gonzalez-Doncel, M., San Segundo, L., Sastre, S., Tarazona, J.V., Torija, C.F., 2011.
1062 Dynamics of BNF-induced in vivo ethoxyresorufin-O-deethylase (EROD) activity during
1063 embryonic development of medaka (Oryzias latipes). Aquat. toxicol. 105, 421-427.
1064 Guinamard, R., Hof, T., Del Negro, C.A., 2014. The TRPM4 channel inhibitor 9-phenanthrol.
1065 Br J Pharmacol 171, 1600-1613.
1066 Hall, T.E., Cole, N.J., Johnston, I.A., 2003. Temperature and the expression of seven muscle-
1067 specific protein genes during embryogenesis in the Atlantic cod Gadus morhua L. J. Exp. Biol.
1068 206, 3187-3200.
1069 Hall, T.E., Smith, P., Johnston, I.A., 2004. Stages of embryonic development in the Atlantic
1070 cod Gadus morhua. J Morphol 259, 255-270.
1071 Hansen, B.H., Salaberria, I., Read, K.E., Wold, P.A., Hammer, K.M., Olsen, A.J., Altin, D.,
1072 Overjordet, I.B., Nordtug, T., Bardal, T., Kjorsvik, E., 2019. Developmental effects in fish
1073 embryos exposed to oil dispersions - The impact of crude oil micro-droplets. Mar Environ Res
1074 150.
1075 Hansen, B.H., Sorensen, L., Carvalho, P.A., Meier, S., Booth, A.M., Altin, D., Farkas, J.,
1076 Nordtug, T., 2018. Adhesion of mechanically and chemically dispersed crude oil droplets to

1077 eggs of Atlantic cod (Gadus morhua) and haddock (Melanogrammus aeglefinus). The Science
1078 of the total environment 640-641, 138-143.
1079 Heintz, R.A., Rice, S.D., Wertheimer, A.C., Bradshaw, R.F., Thrower, F.P., Joyce, J.E., Short,
1080 J.W., 2000. Delayed effects on growth and marine survival of pink salmon Oncorhynchus
1081 gorbuscha after exposure to crude oil during embryonic development. Mar. Ecol. Prog. Ser.
1082 208, 205-216.
1083 Hicken, C.E., Linbo, T.L., Baldwin, D.H., Willis, M.L., Myers, M.S., Holland, L., Larsen, M.,
1084 Stekoll, M.S., Rice, S.D., Collier, T.K., Scholz, N.L., Incardona, J.P., 2011. Sublethal exposure
1085 to crude oil during embryonic development alters cardiac morphology and reduces aerobic
1086 capacity in adult fish. P Natl Acad Sci USA 108, 7086-7090.
1087 Hiroi, J., Miyazaki, H., Katoh, F., Ohtani-Kaneko, R., Kaneko, T., 2005. Chloride turnover and
1088 ion-transporting activities of yolk-sac preparations (yolk balls) separated from Mozambique
1089 tilapia embryos and incubated in freshwater and seawater. J. Exp. Biol. 208, 3851-3858.
1090 Hirose, S., Kaneko, T., Naito, N., Takei, Y., 2003. Molecular biology of major components of
1091 chloride cells. Comp. Biochem. Phys. B 136, 593-620.
1092 Hodson, P.V., 2017. The Toxicity to Fish Embryos of PAH in Crude and Refined Oils. Archives
1093 of environmental contamination and toxicology 73, 12-18.
1094 Hou, J.W., Fei, Y.D., Li, W., Chen, Y.H., Wang, Q., Xiao, Y., Wang, Y.P., Li, Y.G., 2018. The
1095 transient receptor potential melastatin 4 channel inhibitor 9-phenanthrol modulates cardiac
1096 sodium channel. Br J Pharmacol 175, 4325-4337.
1097 Huang, J.H., Elicker, J., Bowens, N., Liu, X., Cheng, L., Cappola, T.P., Zhu, X.H., Parmacek,
1098 M.S., 2012. Myocardin regulates BMP10 expression and is required for heart development. J
1099 Clin Invest 122, 3678-3691.
1100 Hyzd'alova, M., Pivnicka, J., Zapletal, O., Vazquez-Gomez, G., Matthews, J., Neca, J.,
1101 Pencikova, K., Machala, M., Vondracek, J., 2018. Aryl Hydrocarbon Receptor-Dependent
1102 Metabolism Plays a Significant Role in Estrogen-Like Effects of Polycyclic Aromatic
1103 Hydrocarbons on Cell Proliferation. Toxicological sciences : an official journal of the Society
1104 of Toxicology 165, 447-461.
1105 Incardona, J.P., 2017. Molecular Mechanisms of Crude Oil Developmental Toxicity in Fish.
1106 Archives of environmental contamination and toxicology 73, 19-32.
1107 Incardona, J.P., Carls, M.G., Day, H.L., Sloan, C.A., Bolton, J.L., Collier, T.K., Scholz, N.L.,
1108 2009. Cardiac arrhythmia is the primary response of embryonic Pacific herring (*Clupea pallasi*)
1109 exposed to crude oil during weathering. Environmental Science and Technology 43, 201-207.
1110 Incardona, J.P., Carls, M.G., Teraoka, H., Sloan, C.A., Collier, T.K., Scholz, N.L., 2005. Aryl
1111 hydrocarbon receptor-independent toxicity of weathered crude oil during fish development.
1112 Environ. Health Perspect. 113, 1755-1762.
1113 Incardona, J.P., Collier, T.K., Scholz, N.L., 2004. Defects in cardiac function precede
1114 morphological abnormalities in fish embryos exposed to polycyclic aromatic hydrocarbons.
1115 Toxicology and applied pharmacology 196, 191-205.
1116 Incardona, J.P., Gardner, L. P., Linbo, T.L., Brown, T.L., Esbaugh, A.J., Mager, E.M., Stieglitz,
1117 J.D., French, B.L., Labenia, J.S., Laetz, C.A., Tagal, M., Sloan, C.A., Elizur, A., Benetti, D.D.,
1118 Grosell, M., Block, B.A., Scholz, N.L.,, 2014. *Deepwater Horizon* crude oil impacts the
1119 developing hearts of large predatory pelagic fish. P Natl Acad Sci USA.
1120 Incardona, J.P., Scholz, N.L., 2016. The influence of heart developmental anatomy on
1121 cardiotoxicity-based adverse outcome pathways in fish. Aquat. toxicol. 177, 515-525.
1122 Kamelia, L., de Haan, L., Ketelslegers, H.B., Rietjens, I., Boogaard, P.J., 2019. In vitro prenatal
1123 developmental toxicity induced by some petroleum substances is mediated by their 3- to 7-ring
1124 PAH constituent with a potential role for the aryl hydrocarbon receptor (AhR). Toxicol Lett
1125 315, 64-76.

1126 Kamelia, L., Louisse, J., de Haan, L., Rietjens, I., Boogaard, P.J., 2017. Prenatal developmental
1127 toxicity testing of petroleum substances: Application of the mouse embryonic stem cell test
1128 (EST) to compare in vitro potencies with potencies observed in vivo. Toxicol In Vitro 44, 303-
1129 312.
1130 Kimmel, C.B., Miller, C.T., Moens, C.B., 2001. Specification and morphogenesis of the
1131 zebrafish larval head skeleton. Dev. Biol. 233, 239-257.
1132 Kimura, Y., Morita, S.Y., Matsuo, M., Ueda, K., 2007. Mechanism of multidrug recognition
1133 by MDR1/ABCB1. Cancer Sci 98, 1303-1310.
1134 Kuhnert, A., Vogs, C., Seiwert, B., Aulhorn, S., Altenburger, R., Hollert, H., Kuster, E., Busch,
1135 W., 2017. Biotransformation in the zebrafish embryo -temporal gene transcription changes of
1136 cytochrome P450 enzymes and internal exposure dynamics of the AhR binding xenobiotic
1137 benz[a]anthracene. Environ Pollut 230, 1-11.
1138 Laurel, B.J., Copeman, L.A., Iseri, P., Spencer, M.L., Hutchinson, G., Nordtug, T., Donald,
1139 C.E., Meier, S., Allan, S.E., Boyd, D.T., Ylitalo, G.M., Cameron, J.R., French, B.L., Linbo,
1140 T.L., Scholz, N.L., Incardona, J.P., 2019. Embryonic crude oil exposure impairs growth and
1141 lipid allocation in a keystone arctic forage fish. iScience.
1142 Li, F., Zhu, W.F., Gonzalez, F.J., 2017. Potential role of CYP1B1 in the development and
1143 treatment of metabolic diseases. Pharmacol Therapeut 178, 18-30.
1144 Lie, K.K., Meier, S., Sørhus, E., Edvardsen, R.B., Karlsen, O., Olsvik, P.A., 2019. Offshore
1145 Crude Oil Disrupts Retinoid Signaling and Eye Development in Larval Atlantic Haddock. Front
1146 Mar Sci 6.
1147 Lombardo, V.A., Heise, M., Moghtadaei, M., Bornhorst, D., Manner, J., Abdelilah-Seyfried,
1148 S., 2019. Morphogenetic control of zebrafish cardiac looping by Bmp signaling. Development
1149 146.
1150 Magnuson, J.T., Khursigara, A.J., Allmon, E.B., Esbaugh, A.J., Roberts, A.P., 2018. Effects of
1151 Deepwater Horizon crude oil on ocular development in two estuarine fish species, red drum
1152 (Sciaenops ocellatus) and sheepshead minnow (Cyprinodon variegatus). Ecotoxicology and
1153 environmental safety 166, 186-191.
1154 Marris, C.R., N., K.S., Miller, M.R., Incardona, J.P., Brette, F., C., H.J., Sørhus, E., Shiels,
1155 H.A., 2019. Polyaromatic hydrocarbons in pollution: a heart-breaking matter. J. Physiol. 598,
1156 227-247.
1157 McGruer, V., Pasparakis, C., Grosell, M., Stieglitz, J.D., Benetti, D.D., Greer, J.B., Schlenk,
1158 D., 2019. Deepwater Horizon crude oil exposure alters cholesterol biosynthesis with
1159 implications for developmental cardiotoxicity in larval mahi-mahi (Coryphaena hippurus).
1160 Comp Biochem Phys C 220, 31-35.
1161 Meador, J.P., Nahrgang, J., 2019. Characterizing Crude Oil Toxicity to Early-Life Stage Fish
1162 Based On a Complex Mixture: Are We Making Unsupported Assumptions? Environ. Sci.
1163 Technol. 53, 11080-11092.
1164 Miyanishi, H., Okubo, K., Kaneko, T., Takei, Y., 2013. Role of cardiac natriuretic peptides in
1165 seawater adaptation of medaka embryos as revealed by loss-of-function analysis. American
1166 Journal of Physiology - Renal Physiology 304, R423-R434.
1167 Moorthy, B., Chu, C., Carlin, D.J., 2015. Polycyclic aromatic hydrocarbons: from metabolism
1168 to lung cancer. Toxicological sciences : an official journal of the Society of Toxicology 145, 5-
1169 15.
1170 Morrison, C., Bird, C., O'Neil, D., Leggiadro, C., Martin-Robichaud, D., Rommens, M.,
1171 Waiwood, K., 1999. Structure of the egg envelope of the haddock, *Melanogrammus aeglefinus*,
1172 and effects of microbial colonization during incubation. Can J Zool 77, 890-901.
1173 Mu, J., Jin, F., Wang, J., Wang, Y., Cong, Y., 2016. The effects of CYP1A inhibition on alkyl-
1174 phenanthrene metabolism and embryotoxicity in marine medaka (Oryzias melastigma).
1175 Environ Sci Pollut Res Int 23, 11289-11297.

Nebert, D.W., Dalton, T.P., Okey, A.B., Gonzalez, F.J., 2004. Role of aryl hydrocarbon receptor-mediated induction of the CYP1 enzymes in environmental toxicity and cancer. The Journal of biological chemistry 279, 23847-23850.
Nordtug, T., Olsen, A.J., Altin, D., Meier, S., Overrein, I., Hansen, B.H., Johansen, O., 2011. Method for generating parameterized ecotoxicity data of dispersed oil for use in environmental modelling. Mar. Pollut. Bull. 62, 2106-2113.
Olsen, E., Aanes, S., Mehl, S., Holst, J.C., Aglen, A., Gjosaeter, H., 2010. Cod, haddock, saithe, herring, and capelin in the Barents Sea and adjacent waters: a review of the biological value of the area. Ices J Mar Sci 67, 87-101.
Oppen-Berntsen, D.O., Helvik, J.V., Walther, B.T., 1990. The major structural proteins of cod (Gadus morhua) eggshells and protein crosslinking during teleost egg hardening. Dev. Biol. 137, 258-265.
Pampanin, D.M., Kemppainen, E.K., Skogland, K., Jorgensen, K.B., Sydnes, M.O., 2016. Investigation of fixed wavelength fluorescence results for biliary metabolites of polycyclic aromatic hydrocarbons formed in Atlantic cod (Gadus morhua). Chemosphere 144, 1372-1376.
Pangrekar, J., Kole, P.L., Honey, S.A., Kumar, S., Sikka, H.C., 2003. Metabolism of phenanthrene by brown bullhead liver microsomes. Aquatic toxicology (Amsterdam, Netherlands) 64, 407-418.
Pasparakis, C., Esbaugh, A.J., Burggren, W., Grosell, M., 2019. Impacts of deepwater horizon oil on fish. Comparative biochemistry and physiology. Toxicology & pharmacology : CBP 224, 108558.
Pasparakis, C., Mager, E.M., Stieglitz, J.D., Benetti, D., Grosell, M., 2016. Effects of Deepwater Horizon crude oil exposure, temperature and developmental stage on oxygen consumption of embryonic and larval mahi-mahi (Coryphaena hippurus). Aquat. toxicol. 181, 113-123.
Pasparakis, C., Sweet, L.E., Stieglitz, J.D., Benetti, D., Casente, C.T., Roberts, A.P., Grosell, M., 2017. Combined effects of oil exposure, temperature and ultraviolet radiation on buoyancy and oxygen consumption of embryonic mahi-mahi, &ITCoryphaena hippurus&IT. Aquat. toxicol. 191, 113-121.
Pencikova, K., Ciganek, M., Neca, J., Illes, P., Dvorak, Z., Vondracek, J., Machala, M., 2019. Modulation of endocrine nuclear receptor activities by polyaromatic compounds present in fractionated extracts of diesel exhaust particles. The Science of the total environment 677, 626-636.
Petersen, G.I., Kristensen, P., 1998. Bioaccumulation of lipophilic substances in fish early life stages. Environmental Toxicology and Chemistry 17, 1385-1395.
Rottbauer, W., Baker, K., Wo, Z.G., Mohideen, M.A.P.K., Cantiello, H.F., Fishman, M.C., 2001. Growth and function of the embryonic heart depend upon the cardiac-specific L-type calcium channel alpha 1 subunit. Dev Cell 1, 265-275.
Schrlau, J.E., Kramer, A.L., Chlebowski, A., Truong, L., Tanguay, R.L., Simonich, S.L.M., Semprini, L., 2017. Formation of Developmentally Toxic Phenanthrene Metabolite Mixtures by Mycobacterium sp. ELW1. Environ. Sci. Technol. 51, 8569-8578.
Scott, J.A., Incardona, J.P., Pelkki, K., Shepardson, S., Hodson, P.V., 2011. AhR2-mediated, CYP1A-independent cardiovascular toxicity in zebrafish (Danio rerio) embryos exposed to retene. Aquat. Toxicol. 101, 165-174.
Sette, C.B., Pedrete Tde, A., Felizzola, J., Nudi, A.H., Scofield Ade, L., Wagener Ade, L., 2013. Formation and identification of PAHs metabolites in marine organisms. Mar Environ Res 91, 2-13.
Shelbourne, J.E., 1957. Site of Chloride Regulation in Marine Fish Larvae. Nature 180, 920-922.

Shou, W., Aghdasi, B., Armstrong, D., Guo, Q., Bao, S., Charng, M., Mathews, L., Schneider, M., Hamilton, S., Matzuk, M., 1998. FKBP12-deficient mice exhibit congenital dilated cardiomyopathy and altered ryanodine receptor function. Biophys J 74, A353-A353.

Shwartz, Y., Farkas, Z., Stern, T., Aszodi, A., Zelzer, E., 2012. Muscle contraction controls skeletal morphogenesis through regulation of chondrocyte convergent extension. Dev. Biol. 370, 154-163.

Sievers, C.K., Shanle, E.K., Bradfield, C.A., Xu, W., 2013. Differential action of monohydroxylated polycyclic aromatic hydrocarbons with estrogen receptors alpha and beta. Toxicological sciences : an official journal of the Society of Toxicology 132, 359-367.

Solemdal, P., Mukhina, N., Knutsen, T., Bjørke, H., Fossum, P., 1997. Maturation, spawning and egg drift of Arcto-Norwegian haddock (*Melanogrammus aeglefinus*), Icthyoplankton Ecology. University college Galway, Ireland.

Sorensen, L., Hansen, B.H., Farkas, J., Donald, C.E., Robson, W.J., Tonkin, A., Meier, S., Rowland, S.J., 2019. Accumulation and toxicity of monoaromatic petroleum hydrocarbons in early life stages of cod and haddock. Environ Pollut 251, 212-220.

Sørensen, L., Sørhus, E., Nordtug, T., Incardona, J.P., Linbo, T.L., Giovanetti, L., Karlsen, O., Meier, S., 2017. Oil droplet fouling and differential toxicokinetics of polycyclic aromatic hydrocarbons in embryos of Atlantic haddock and cod. Plos One 12, e0180048.

Sørhus, E., Edvardsen, R.B., Karlsen, O., Nordtug, T., van der Meeren, T., Thorsen, A., Harman, C., Jentoft, S., Meier, S., 2015. Unexpected interaction with dispersed crude oil droplets drives severe toxicity in atlantic haddock embryos. Plos One 10, e0124376.

Sørhus, E., Incardona, J.P., Furmanek, T., Goetz, G.W., Scholz, N.L., Meier, S., Edvardsen, R.B., Jentoft, S., 2017. Novel adverse outcome pathways revealed by chemical genetics in a developing marine fish. Elife 6.

Sørhus, E., Incardona, J.P., Furmanek, T., Jentoft, S., Meier, S., Edvardsen, R.B., 2016a. Developmental transcriptomics in Atlantic haddock: Illuminating pattern formation and organogenesis in non-model vertebrates. Dev. Biol. 411, 301-313.

Sørhus, E., Incardona, J.P., Karlsen, O., Linbo, T., Sørensen, L., Nordtug, T., van der Meeren, T., Thorsen, A., Thorbjørnsen, M., Jentoft, S., Edvardsen, R.B., Meier, S., 2016b. Crude oil exposures reveal roles for intracellular calcium cycling in haddock craniofacial and cardiac development. Sci. Rep. 6, 31058.

Sun, L.B., Ruan, J.P., Lu, M.C., Chen, M., Dai, Z.L., Zuo, Z.H., 2019. Combined effects of ocean acidification and crude oil pollution on tissue damage and lipid metabolism in embryo-larval development of marine medaka (Oryzias melastigma). Environ Geochem Hlth 41, 1847-1860.

Ta, C.M., Adomaviciene, A., Rorsman, N.J., Garnett, H., Tammaro, P., 2016. Mechanism of allosteric activation of TMEM16A/ANO1 channels by a commonly used chloride channel blocker. Br J Pharmacol 173, 511-528.

Thisse, C., Thisse, B., 2008. High-resolution in situ hybridization to whole-mount zebrafish embryos. Nature protocols 3, 59-69.

Thrane, V.R., Thrane, A.S., Wang, F.S., Cotrina, M.L., Smith, N.A., Chen, M., Xu, Q.W., Kang, N., Fujita, T., Nagelhus, E.A., Nedergaard, M., 2013. Ammonia triggers neuronal disinhibition and seizures by impairing astrocyte potassium buffering. Nat Med 19, 1643-1648.

Timme-Laragy, A.R., Noyes, P.D., Buhler, D.R., Di Giulio, R.T., 2008. CYP1B1 knockdown does not alter synergistic developmental toxicity of polycyclic aromatic hydrocarbons in zebrafish (Danio rerio). Mar Environ Res 66, 85-87.

Valen, R., Eilertsen, M., Edvardsen, R.B., Furmanek, T., Ronnestad, I., van der Meeren, T., Karlsen, O., Nilsen, T.O., Helvik, J.V., 2016. The two-step development of a duplex retina involves distinct events of cone and rod neurogenesis and differentiation. Dev. Biol. 416, 389-401.

1275 Van de Wiele, T., Vanhaecke, L., Boeckaert, C., Peru, K., Headley, J., Verstraete, W., Siciliano,
1276 S., 2005. Human colon microbiota transform polycyclic aromatic hydrocarbons to estrogenic
1277 metabolites. Environ. Health Perspect. 113, 6-10.
1278 Vandenberg, J.I., Perry, M.D., Perrin, M.J., Mann, S.A., Ke, Y., Hill, A.P., 2012. hERG K(+)
1279 channels: structure, function, and clinical significance. Physiol. Rev. 92, 1393-1478.
1280 Vanleeuwen, C.J., Griffioen, P.S., Vergouw, W.H.A., Maasdiepeveen, J.L., 1985. Differences
1281 in Susceptibility of Early Life Stages of Rainbow-Trout (Salmo-Gairdneri) to Environmental-
1282 Pollutants. Aquat. toxicol. 7, 59-78.
1283 Wamhoff, B.R., Bowles, D.K., McDonald, O.G., Somlyo, A.P., Somlyo, A.S., Owens, G.K.,
1284 2004. L-type voltage-gated Ca2+ channels modulate expression of smooth muscle
1285 differentiation marker genes via a Rho kinase/myocardin/SRF-dependent mechanism.
1286 Circulation 110, 261-261.
1287 Wamhoff, B.R., Bowles, D.K., Owens, G.K., 2006. Excitation-transcription coupling in arterial
1288 smooth muscle. Circ. Res. 98, 868-878.
1289 Wang, Y., Pasparakis, C., Mager, E.M., Stieglitz, J.D., Benetti, D., Grosell, M., 2019. Ontogeny
1290 of urea and ammonia transporters in mahi-mahi (Coryphaena hippurus) early life stages.
1291 Comparative Biochemistry and Physiology a-Molecular & Integrative Physiology 229, 18-24.
1292 Wells, P.G., Kim, P.M., Laposa, R.R., Nicol, C.J., Parman, T., Winn, L.M., 1997. Oxidative
1293 damage in chemical teratogenesis. Mutation research 396, 65-78.
1294 Wells, P.G., McCallum, G.P., Chen, C.S., Henderson, J.T., Lee, C.J.J., Perstin, J., Preston, T.J.,
1295 Wiley, M.J., Wong, A.W., 2009. Oxidative Stress in Developmental Origins of Disease:
1296 Teratogenesis, Neurodevelopmental Deficits, and Cancer. Toxicological Sciences 108, 4-18.
1297 Williams, A.L., Eason, J., Chawla, B., Bohnsack, B.L., 2017. Cyp1b1 Regulates Ocular Fissure
1298 Closure Through a Retinoic Acid-Independent Pathway. Invest Ophth Vis Sci 58.
1299 Wincent, E., Jonsson, M.E., Bottai, M., Lundstedt, S., Dreij, K., 2015. Aryl Hydrocarbon
1300 Receptor Activation and Developmental Toxicity in Zebrafish in Response to Soil Extracts
1301 Containing Unsubstituted and Oxygenated PAHs. Environmental Science and Technology 49,
1302 3869-3877.
1303 Xu, E.G.B., Mager, E.M., Grosell, M., Hazard, E.S., Hardiman, G., Schlenk, D., 2017. Novel
1304 transcriptome assembly and comparative toxicity pathway analysis in mahi-mahi (Coryphaena
1305 hippurus) embryos and larvae exposed to Deepwater Horizon oil. Sci. Rep. 7.
1306 Yamamoto, Y., Zolfaghari, R., Ross, A.C., 2000. Regulation of CYP26 (cytochrome P450RAI)
1307 mRNA expression and retinoic acid metabolism by retinoids and dietary vitamin A in liver of
1308 mice and rats. Faseb J 14, 2119-2127.
1309 Yin, H.C., Tseng, H.P., Chung, H.Y., Ko, C.Y., Tzou, W.S., Buhler, D.R., Hu, C.H., 2008.
1310 Influence of TCDD on zebrafish CYP1B1 transcription during development. Toxicological
1311 Sciences 103, 158-168.
1312 Zimmer, A.M., Brauner, C.J., Wood, C.M., 2014. Ammonia transport across the skin of adult
1313 rainbow trout (Oncorhynchus mykiss) exposed to high environmental ammonia (HEA). J Comp
1314 Physiol B 184, 77-90.
1315 Zimmer, A.M., Wright, P.A., Wood, C.M., 2017. Ammonia and urea handling by early life
1316 stages of fishes. J. Exp. Biol. 220, 3843-3855.
1317